Journal of Cosmology, 2010, Vol 6, 1438-1472
Cosmology, February 15, 2010

Does Sgr A* Have an Event Horizon or a Magnetic Moment?

Stanley L. Robertson, Ph.D.[1], and Darryl J. Leiter, Ph.D.[2],

[1]Physics Dept., Southwestern Oklahoma State University, Weatherford, OK 73096, USA

[2]Visiting Scientist, National Radio Astronomy Observatory
Charlottesville, VA 22903, USA

Abstract

In this work we extend the general relativistic Magnetospheric Eternally Collapsing Object (MECO) model for application to Sgr A*. In a series of papers published within the last few years, it has been shown that the MECO model has been able to account for all of the observational phenomena associated with the galactic black hole candidates (GBHC) and more luminous active galactic nuclei (AGN). For a given mass, the MECO is characterized by only two mass scaled parameters; surface magnetic field strength and rotation rate. Without changing either of these parameters previously found for GBHC and AGN, we demonstrate that the MECO model for Sgr A*: a) satisfies all of the luminosity constraints that have previously been claimed as proof of an event horizon, b) reconciles the low bolometric luminosity of Sgr A* with its expected Bondi accretion rate by means of a magnetic propeller driven outflow, c) accounts for the Sgr A* NIR and X-ray luminosities, the general characteristics of its broad band spectrum, and the temporal sequence of flares in different spectral ranges as well as the pattern of its observed orthogonal radio and NIR polarizations. High resolution radio images of a MECO would be produced in an equatorial OUTFLOW, while high resolution images in NIR wavelengths would be elongated along two INFLOWS into the magnetic poles (apparently generally N-S). These patterns would be distinguishable from black hole RIAF models for which all emissions would arise from an accretion disk. Combination black hole disk-jet models for which the NIR originated in a disk viewed at high inclination would also be distinguished by showing only unidirectional flow.

Key Words: accretion, accretion disks–black hole physics–Galaxy : center–gravitation–infrared: general–magnetic fields

1 Introduction

The pointed question stated in the title of this paper represents the beginning of a clear test for the existence or the non-existence of a black hole at the galactic center location of Sgr A*. In previous papers we have described a fully general relativistic model for a highly redshifted Magnetospheric Eternally Collapsing Object (MECO) that is compact enough to be a black hole but does **NOT** possess an event horizon. As recapitulated in

appendixes here, it is a particular model within the class of eternally collapsing objects (ECO) (Mitra 2006a,b,c,). Such objects, of arbitrary mass, can exist within the context of General Relativity. Stellar mass and larger ECO continue gravitational collapse over lifetimes that can greatly exceed a Hubble time while stabilized via the mechanism of an Eddington balance. Such a balance requires a very hot radiating interior, but it must be combined with a large gravitational redshift that is capable of reducing its apparent luminosity to within observational limits. The physical nature of the interior is an active research topic (e.g., Mitra & Glendenning 2010 and references therein), however, some structural features can be discerned. Decreasing temperatures in the outer layers should permit the existence of free baryons as well as a region further out that is rich in electron-positron pairs.

The MECO has a very strong intrinsic magnetic moment, which is an attribute that cannot be possessed by a black hole. If such a MECO object exists at the center of our galaxy at Sgr A*, its strong magnetic field and slow rate of rotation should produce easily observed effects on its accretion environment that would uniquely distinguish it from a black hole. Spatial and broadband spectral radiation distributions as well as their polarizations should be dominated by the MECO magnetic field. If these effects are not observed we would be able to conclude that Sgr A* does not possess an intrinsic magnetic moment, which would take us one step closer to concluding that it is a genuine black hole. However this remains an open question since currently existing observations do not yet contradict the idea that Sgr A* might be intrinsically magnetic. The massive compact object at the center of our galaxy in Sgr A* has been observed with increasing resolution in wavelengths from x-rays to radio. Recent observations have shown detail on scales approaching that of the event horizon of a black hole of the mass of Sgr A*. Observations planned for the near future are generating great excitement at the prospect of obtaining images of the shadow of the event horizon. In this paper we will discuss these observations of Sgr A* and try to identify ways in which a MECO might be distinguished from a black hole.

The luminosity of Sgr A* is believed to be powered by accretion, requiring a minimum accretion rate of about $2 \times 10^{-10} M_{\odot}\ yr^{-1}$ to produce $\sim 10^{36}$ erg s^{-1}, however, the polarization of emissions sets an upper limit of about $10^{-9} M_{\odot}\ yr^{-1}$ that can get within a few gravitational radii (GM/c^2) of Sgr A*, modeled as a black hole (Agol 2000). On the other hand, it has been estimated that the environment of Sgr A* should provide plasma for a Bondi accretion rate of about $3 \times 10^{-6} M_{\odot}\ yr^{-1}$ (Baganoff et al. 2003). Thus there must be both inflow and outflow of accreting material with the great bulk of the plasma escaping. It is not presently known how escape is achieved, but it must occur beyond a few tens of gravitational radii or the flow would likely produce more luminosity than is observed. This is an important constraint on models for Sgr A*.

With a mass of $4.5 \pm 0.4 \times 10^6 M_{\odot}$ at a distance of $8.4 \pm 0.4\ kpc$, (Ghez et al. 2008) an object the angular size of the event horizon for a mass as large as Sgr A* would be $21 \mu as$. Its self-lensed image would be larger at $\sim 55 \mu as$. Surprisingly, recent VLBI radio observations at 230 GHz are consistent with an object of approximately half this size (Doeleman et al. 2008). This strongly implies that the accretion flow is structured and Sgr A* is not simply enveloped in luminous accreting plasma. With observations in the NIR capable of revealing flow directions at a resolution of $10 \mu as$ planned for the near future (Eisenhaur et al 2008) we can soon expect to see some interesting images of Sgr A*. The question is, might we see anything that could be distinguished from a black hole?

In this work we describe some of the observational characteristics to be expected for a strongly magnetic and slowly rotating compact object at the location of Sgr A*. We show that such an object is consistent with observations of Sgr A* to date, but that it should be distinguishable from a black hole in future observations. The MECO model for galactic black hole candidates (GBHC) and active galactic nuclei (AGN) is fully general relativistic and has been previously described (Leiter & Robertson 2003, Robertson & Leiter 2003, 2004, 2006, hereafter RL03, RL04, RL06, Schild, Leiter & Robertson 2006, 2008). For the convenience of readers, we recapitulate some of the properties of both ECO and MECO in appendixes. We have previously provided some evidence for the existence of magnetic moments for both GBHC (Robertson & Leiter 2002, hereafter RL02) and AGN (Schild, Leiter & Robertson 2006, 2008). Others have reported evidence for very strong magnetic fields in GBHC. The field in excess of 10^8 G that has been found at the base of the jets of GRS 1915+105 (Gliozzi, Bodo & Ghisellini 1999, Vadawale, Rao & Chakrabarti 2001) is likely in excess of what can be produced by an equipartition accretion disk. Whatever their origins, magnetic fields and their synchrotron radiations are ubiquitous among the black hole candidates. They likely play an important role in the structure of the accretion flow into Sgr A*. Since intrinsic magnetic moments are forbidden attributes for black holes, there would be important consequences for astrophysics if a black hole candidate were found to possess one. In the MECO model of Sgr A*, the bulk of the Bondi accretion flow is expelled in a magnetic propeller driven outflow. Only a small fraction of the Bondi flow reaches the central MECO. The luminosities originating in these two parts of the flow must be considered separately.

2 MECO "Surface" Emissions and SGR A* Low Luminosity Constraints

A MECO avoids rapid collapse to a black hole state by radiating away its mass-energy at an Eddington limit rate. It is characterized by both an extreme redshift and a strong intrinsic magnetic moment (see Appendix A - C). The large redshift can account for the low quiescent surface luminosities of GBHC and AGN and their extremely long (many Hubble times) radiative lifetimes. It has been pointed out previously (Abramowicz, Kluzniak & Lasota 2002) that proving the existence of event horizons might be very difficult if objects with sufficiently large surface gravitational redshift exist. Extreme redshifts could make such objects essentially as dark as a black hole (see Appendixes A - D). On the other hand if the intrinsically magnetic effects associated with a MECO could be ruled out, there would presumably be no remaining astrophysical alternatives to black holes. The MECO model is consistent with the lower limit on the quiescent emission from the GBHC XTE J1118+480 (McClintock, Narayan & Rybicki 2004). In addition, its highly red shifted Eddington limited baryon surface is a phase transition zone at the base of an electron-positron atmosphere and not a "hard surface". We show below that the MECO model is consistent with the low luminosity constraints observed for Sgr A* (Broderick and Narayan 2006, hereafter BNO6, Broderick, Loeb & Narayan 2009, hereafter BLN09)

For the extreme redshift of the MECO, the photosphere of its pair atmosphere lies deep within the photon sphere (see Appendix A, B, C). The photosphere is the last scattering surface of the pair plasma atmosphere, however, it should be noted that the

escape cone from the photosphere is so small that most of the photons that arrive there still do not escape. The pair atmosphere is maintained in part by a magnetic field of $\sim 10^{20}$ G (RLO3)which is strong enough to create bound pairs (Harding 2003, Zaumen, 1976) on a deeper lying baryon surface. The interior magnetic field is much smaller, as required by the Maxwell-Einstein boundary condition (see Appendix B). The ratio of surface to interior magnetic field strength is what determines the MECO redshift for the mass of Sgr A* to to be $(1+z_s) \sim 10^{11}$. In addition, the compactness of Sgr A* yields a ratio of surface luminosity to radius that is 5×10^{13} times larger than the $L/R \sim 10^{30}$ erg s^{-1} cm^{-1} for which photon-photon collisions yield copious pair production (Cavaliere & Morrison 1980). Between the extremes of pure magnetic energy, which does not collapse into a black hole state (Thorne 1965) and polytropic gases or dust which may, it is possible to stabilize the MECO collapse rate at the Eddington limit (RL03, RL06). The base of the pair atmosphere is a phase transition zone. Photon-photon collisions and pair production keep the temperature there buffered at approximately the pair production threshold of $\sim 6\times10^9$ K (RL03). For the mass of Sgr A*, the photosphere temperature and redshift would be 3×10^8 K and 3.5×10^5, respectively (Appendix C and Table 2).

Accreting baryonic matter that reaches the pair atmosphere photosphere can lose energy via Coulomb scattering of electrons and positrons and Compton scattering of photons. It would eventually be brought to rest and its energy deposited in the phase transition zone at the base of the pair atmosphere. At the photosphere the effect would be like a cannonball fired into a dust cloud. At the baryon surface, it would be more like water falling onto the surface of a liquid and not at all like a hard surface collision. For conditions in the pair atmosphere (see Appendix D) only about 10^{-13} of the accretion energy could escape from the photosphere to be observed distantly (and further redshifted). Most of the accretion energy released is therefore absorbed below the MECO baryon surface which is covered by an extremely optically thick layer of pairs for which the escape cone is negligibly small. The adjustment to additional mass reaching the baryon zone of the MECO would take place on a local acoustic wave proper time scale of $\sim 2R_g/c \sim 44$ s. We can contrast this with the much longer time that would be required for photons produced there to diffuse through the pair atmosphere. The average pair density is about $n \sim 10^{29}$ cm^{-3} (see Appendix C) and the mean free path of a photon is about $l_p = (n\sigma_T)^{-1} \sim 1.5\times10^{-5}$ cm, where $\sigma_T = 6.6\times10^{-25}$ cm^2 is the Thompson cross-section. The diffusion coefficient for photons would thus be about $D = l_p c/3 \sim 1.5\times10^5$ cm^2 s^{-1}. The proper length thickness of the pair atmosphere is about $l = \int dr(1+z) \approx 4R_g/(1+z_p) = 8\times10^6$ cm, where $R_g = 6.7\times10^{11}$ cm is the gravitational radius (see Table 2) and $(1+z_p) = 3.5\times10^5$ is the redshift at the photosphere (Appendix C). The proper time for photons to diffuse from the baryon surface through the photosphere would be about $t \sim l^2/6D = 7\times10^7$ s. Thus the MECO has ample time to adjust to any additional accreted mass that it acquires without requiring that it be radiated away. Further, radiation from a surface accretion event could only appear externally on a much longer time scale of about $(7\times10^7\ s)(1+z_s) \sim 10^{12}$ yr, where $(1+z_s) = 1.2\times10^{11}$ is the redshift at the baryon surface. It is safe to say that none of the rapid variability of Sgr A* would originate from a MECO surface. The accretion mass-energy adds to the mass of the MECO and is eventually radiated away with 100% efficiency, but on the timescale of the long MECO radiative lifetime (see Appendix A). Thus the MECO swallows accreting plasma about as effectively as a black hole.

The only thing that is required of the MECO to maintain its stability is for the radiation pressure in the accretion zone to increase by enough to counter the pressure

supplied by accretion. We can examine this requirement by considering an extreme case in which we imagine that the velocity of the accreting matter would be slowed to zero by inelastic collisions with MeV photons and pairs right at the photosphere, from which some radiation might actually have a chance of escaping. Consider a particle of rest mass m_o in radial free fall from infinity. Its speed as it reaches the photosphere would be essentially light speed, c, according to an observer at the photosphere, and it would have a momentum of $\gamma m_o c$, where $\gamma = 1 + z_p$ is the Lorentz factor[1]. If particles arrive at the locally observed rate of dN/dt_p, then the quantity of momentum deposited according to the observer at the photosphere would be $(dN/dt_p)(1+z_p)m_o c$. With the substitution of $dt/(1 + z_p)$ for dt_p, this becomes $(dN/dt)m_o(1 + z_p)^2 c$. Thus the rate of momentum transport, as observed at the photosphere is $\dot{m}_\infty(1 + z_p)^2 c$, where $\dot{m}_\infty = m_o dN/dt$.

If this momentum were deposited uniformly at the photosphere, the accretion pressure would be $p_{accr} = \dot{m}_\infty(1 + z_p)^2 c/(4\pi R^2)$ For the mass of Sgr A* and $\dot{m}_\infty = 2 \times 10^{-9} M_\odot yr^{-1} = 1.3 \times 10^{17} g\ s^{-1}$, (see Section 4 below) this would yield $p_{accr} = 2.2 \times 10^{13}$ erg cm^{-3}. The radiation pressure at the photosphere, for $T_p = 3 \times 10^8$ K, would be $p_{rad} = aT_p^4/3 = 2.2 \times 10^{19}$ erg cm^{-3}. This pressure ratio would be $p_{accr}/p_{rad} = 10^{-6}$, however, the actual ratio of accretion and radiation pressures would be smaller yet by an additional factor of about 10^{-4} because so little of the momentum is actually deposited in the pair atmosphere. Thus the photosphere remains quiescent for an accretion rate appropriate for Sgr A*.

For a quiescent MECO, the observed radiated flux at frequency ν_∞ and distance R ($> 3R_g$) from the MECO is given by (See Appendix A, Eq. 17)

$$F_{\nu_\infty} = \frac{2\pi h \nu_\infty^3}{c^2} \frac{1}{e^{(h\nu_\infty/kT_\infty)} - 1} \frac{27R_g^2}{R^2} \tag{1}$$

For the parameters of Table 2, this would produce a spectral peak at $6\mu m$ with a peak flux of 0.65 mJy. For the most constraining NIR wavelength of $3.8\mu m$ the quiescent MECO flux density given by Eq. 1 is 0.47 mJy, which lies below the observational upper limit (Ghez et al. 2005) by a factor of three. Since the highly red shifted Eddington limited surface of the MECO is not a "hard surface" the validity of this result is not affected by arguments (BN06, BLN09) that attempt to show that Sgr A* must have an event horizon.

3 General MECO Properties and Parameters

The MECO model for disk accreting GBHC and AGN accounts for the existence of their low/hard and high/soft x-ray spectral states. The rotating magnetic moments provide a robust universal magnetic propeller mechanism for spectral state switches (Ilarianov & Sunyaev 1975, Campana et al., 1998, 2002, RL02, RL03). The high/soft → low/hard transition marks the start of a magnetic propeller regime, the end of accreting plasma being able to penetrate inside the corotation radius and the beginning of a low state jet outflow with radio and x-ray luminosities related as $L_R \propto L_x^{2/3}$, as observed (Gallo, Fender & Pooley 2003, Markoff et al. 2003, Falcke, Körding & Markoff 2004, Maccarone, Gallo & Fender 2003). The MECO model correctly predicts (RL04) that this transition

[1]From the geodesic equations of motion, the distant coordinate time, t, and proper time, τ, moving with the particle are related by $dt = (1+z_p)^2 d\tau$. An interval dt_p for an observer at rest at the photosphere is related by $dt_p = \gamma d\tau = dt/(1 + z_p)$, from which it follows that $\gamma = 1 + z_p$

Table 1: MECO Model Equations

MECO Physical Quantity	Equation	Scaling
1. Surface Redshift - (RL06 2)	$1+z_s = 5.67\times10^7 m^{1/2}$	$m^{1/2}$
2. Quiescent Surface Luminosity L_∞ - (RL06 29)	$L_\infty = 1.26\times10^{38} m/(1+z_s)$ erg s^{-1}	$m^{1/2}$
3. Quiescent Surface Temp T_∞ - (RL06 31)	$T_\infty = 2.3\times10^7/[m(1+z_s)]^{1/4} = 2.65\times10^5 m^{-3/8}$ K	$m^{-3/8}$
4. Photosphere Temp. T_p	$T_p = 4.9\times10^8 m^{-0.032}$ K	$m^{-0.032}$
5. Photosphere redshift z_p	$1+z_p = 1840 m^{0.343}$	$m^{0.343}$
6. GBHC Rotation Rate, units 10^2 Hz - (RL06 47)	$\nu_2 = 0.89[L_{q,32}/m]^{0.763}/L_{c,36} \approx 0.6 s_1/m\ Hz^a$	m^{-1}
7. GBHC Quiescent Lum., units 10^{32} erg s^{-1} - (RL06 45, 46)	$L_{q,32} = 1.17[\nu_2 L_{c,36}]^{1.31} = 4.8\times10^{-3}\mu_{27}^{2.62}\nu_2^{5.24} m^{-0.31}$ erg s^{-1}	m
8. Co-rotation Radius - (RL06 40)	$R_c = 7\times10^6[m/\nu_2^2]^{1/3}$ cm	m
9. Low State Luminosity at R_c, units 10^{36} erg s^{-1} (RL06 41)	$L_{c,36} = 0.015\mu_{27,\infty}^2\nu_2^3/m$ erg s^{-1}	m
10. Magnetic Moment, units 10^{27} $G\ cm^3$ - (RL06 41, 47)	$\mu_{27,\infty} = 8.16[L_{c,36} m/\nu_2^3]^{1/2}$ $\mu = 1.7\times10^{28} m^{5/2}$ $G\ cm^3$	$m^{5/2}$
11. Disk Accr. Magnetosphere Radius - (RL06 38)	$r_m(disc) = 8\times10^6[\mu_{27,\infty}^4/(m\dot{m}_{15}^2)]^{1/7}$ cm	m
12. Spherical Accr. Magnetosphere Radius	$r_m(sphere)$ or axial $z_m(in) = 2.3\times10^7[\mu_{27,\infty}^4/(m\dot{m}_{15}^2)]^{1/7}$ cm	m
13. Spher. Accr. Eq. Mag. Rad. Rotating Dipole (RTTL03)	$r_m(out) = 1.2\times10^7[\mu_{27}^2/(\dot{m}_{15}\nu_2)]^{1/5}$ cm	m
14. Equator Poloid. Mag. Field - (RL06 41, 47, $B_\perp = \mu_\infty/r^3$)	$B_{\infty,10} = 250 m^{-3}(R_g/r)^3$ [b] $[L_{c,36}/(m^5\nu_2^3)]^{1/2}$ gauss	$m^{-1/2}$
15. Low State Jet Radio Luminosity - (RL04 18, 19)	$L_{radio,36} = 10^{-6.64} m^{0.84} L_{x,36}^{2/3}[1-(L_{x,36}/L_{c,36})^{1/3}]$ erg s^{-1}	$m^{3/2}$

a: s_1 is a small dimensionless numerical factor ($s_1 \sim 1$ for GBHC, see text)
b: $R_g = GM/c^2$

occurs at about ~ 0.02 of Eddington limit luminosity for both GBHC and AGN. The luminosities at the transition and in quiescence have permitted the determinations of the magnetic moments and spin rates for MECO-GBHC (RL02, RL06, and Eqs 6 & 10, Table 1). Spectral state switches are common to dwarf novae, the neutron stars and GBHC of low mass x-ray binary systems and AGN. They seem to be signatures of intrinsic magnetism, however for the case of the GBHC they have not yet been accepted as such because it is generally believed that the black hole candidates contain actual black holes which cannot possess magnetic moments.

For the discussion to follow and also for the convenience of readers who might wish to relate MECO properties to observations of other objects, we have tabulated a number of useful relations in Table 1. Many of the parameters are given in terms of quiescent x-ray luminosity L_q, or the luminosity, L_c, at the transition high/soft $\rightarrow$ low/hard state since these are often measurable quantities. Some new developments, minor corrections and general features for the MECO model are presented in Appendixes A - E. Mass scaling relationships for MECO are listed in the right hand column of Table 1. They have been shown to account for the newly discovered quasar accretion structures (Schild, Leiter & Robertson 2006, 2008) revealed by microlensing observations of the quasars Q0957+561 and Q2237+0305. The observed structures are consistent with the strongly magnetic MECO model but do not accord with standard thin disk models of accretion flows into a black hole. Since even the nearest GBHC are much too small to be resolved in the detail shown by the microlensing techniques which were used in the study of Q0957 and Q2237, Sgr A* is likely the only remaining black hole candidate for which resolved images might reveal whether or not it possesses a magnetic moment. For this reason it is important that it be tested.

With $m = 4.5\times10^6$ solar as the given mass of Sgr A*, all other parameters for our MECO model except its spin rate have been determined by scaling up from observations of GBHC. We should expect the spin rate to be influenced by angular momentum transported to the MECO by its accretion environment. One would not necessarily expect a low mass binary star system to provide a good analogue for an AGN. Nevertheless, the similar corotation radii $(30-100R_g)$ of disk accreting GBHC and AGN are necessary for consistency with their mass scale independent radio cutoffs at ~ 0.02 of Eddington

Table 2: MECO Parameters for Sgr A*

1. Mass - $m = 4.5 \times 10^6$
2. Surface Redshift - $1 + z_s = 1.2 \times 10^{11}$
3. Quiescent Surface Luminosity $L_\infty = 4.7 \times 10^{33}$ erg s^{-1}
4. Quiescent distantly observed temp $T_\infty = 848$ K
5. Photosphere Temp. $T_p = 3 \times 10^8$ K
6. Photosphere redshift $1 + z_p = 3.5 \times 10^5$
7. Spin Rate, $\nu = 1.33 s_1 \times 10^{-5}$ Hz
8. Co-rotation Radius - $r_c = 4.4 \times 10^{13} s_1^{-2/3}$ cm
9. Axial Magnetopause distance $z_m (in = 1.2 \times 10^{15}$ cm
10. Gravitational Radius - $R_g = 6.7 \times 10^{11}$ cm
11. Magnetic Moment, $\mu = 7.3 \times 10^{44}$ $G\ cm^3$

limit luminosity. Given this mass scale invariant property, it is not surprising that they seem to show little variability in spins that scale as $\nu_s \propto m^{-1}$. For this reason we take the spin to be $\nu_s = 60 s_1/m\ Hz$, where s_1 is a small dimensionless numerical factor to be determined ($s_1 \sim 1$ for GBHC). The other parameters that characterize the MECO model of Sgr A* are shown in Table 2.

Because much of the spectrum of Sgr A* appears to originate in synchrotron-cyclotron radiation, the most stringent tests of the hypothesis that Sgr A* might possess an intrinsic magnetic moment will require global solutions for the magnetic field and electron density distributions for some kind of accretion flow. As with black hole models, a true *ab initio* computation is still well beyond reach (Broderick et al. 2009). Future detailed simulations that are beyond the scope of the present work will be needed, however, the accretion regions from which various MECO emissions would arise are known and we show here that analytic methods can be used to give a good accounting of the physical properties of the radio/NIR and X-ray spectral characteristics, luminosities, polarizations and timing features that have been observed for Sgr A*. We find that we must consider Bondi accretion for a quiescent MECO and then show that we can reconcile the observed low luminosity of Sgr A* with the expected Bondi accretion flow rate.

4 MECO-BONDI INFLOW-OUTFLOW MODEL FOR SGR A*

The multiwavelength spectrum of Sgr A* shows (e.g. An et al. 2005) a relatively flat radio spectrum with a flux density dropping steeply from a few Jy near 1000 GHz to a few mJy in the NIR. The flat radio spectrum has been attributed to compact relativistic plasma within a few R_g of Sgr A*. The similar flat radio spectra for GBHC are thought to arise from a jet outflow (Markoff, Falcke & Fender 2001, Falcke, Körding & Markoff 2003). It has been suggested that there could be a compact jet outflow from Sgr A* (Falcke & Markoff 2000, Yuan, Markoff & Falcke 2002), however there is still a vigorous debate (Fish et al. 2009) over whether the emission of Sgr A* is produced predominantly by a hot accretion disk or from an energetic outflow. In GBHC systems low state GBHC jets have been resolved (Stirling et al. 2001) and studied over a wide range of GBHC

luminosity variation (Corbel et al. 2000, 2003). It has further been shown (RL04, Heinz & Sunyaev 2003) that the radio spectra are consistent with mass scale invariant jets. Whether all (e.g., Heinz & Sunyaev 2003), or only part (RL04), of the low state x-ray emissions of GBHC originate in the base of the jet, it is clear that the base of a jet would contribute.

The quiescent radiation from a MECO model for Sgr A* probably would not originate in a jet outflow from an accretion disk. Although more luminous AGN, modeled as MECO, are largely scaled up versions of disk accreting GBHC, there are differences in quiescence. In true quiescence for the MECO-GBHC the inner disk radius lies beyond the light cylinder. But $T_\infty \approx 10^5\ K$ for a central MECO-GBHC is much higher than for an AGN. Even for a faint quiescent MECO-GBHC there would be a thermal radiation flux capable of ionizing and ablating the inner regions of an accretion disk out to $\sim 5\times10^3 R_g$. Ablated material at low accretion rate would fall in and then be swept out by the rotating magnetic field. This would produce the stochastic power-law soft x-ray emissions in the MECO-GBHC quiescent state. For Sgr A*, there would be only the cooler NIR radiation and insufficient luminosity to ablate an inner disk with radius beyond its light cylinder, hence nothing to keep the inner disk further away. If the luminosity of the true quiescent state for Sgr A* would correspond to a disk with inner radius at the light cylinder, it would be at least as luminous as $L_{q,max} = (2.7\times10^{30}\ ergs^{-1})\mu_{27}^2\nu_2^{9/2}m^{1/2} \sim 3.4\times10^{38}s_1^{9/2}$ erg s^{-1} (see RL06 Eq. 43 and Table 2 for magnetic moment and spin). But since the luminosity of Sgr A* is well below this level, we can conclude that its luminosity does not arise from a conventional optically thick, geometrically thin accretion disk that extends in to the light cylinder. This leaves a Bondi accretion flow as the likely spectral source for a MECO model for Sgr A*.

4.1 Bondi Accretion and Magnetic Propeller Effects

Based on plasma conditions within the central parsec of the galaxy, a Bondi accretion rate of $\dot{m}_\infty = 3\times10^{-6}M_\odot yr^{-1} = 2\times10^{20}\ gs^{-1}$ and sound speed of $c_{s,\infty} = 550\ km\ s^{-1}$ have been estimated (Baganoff et al. 2003). The corresponding Bondi radius is $R_B = GM/c_\infty^2 = 2\times10^{17}\ cm$. This expected accretion rate creates an interesting conundrum. Even without any surface contributions an accretion flow this large should create far more luminosity than is observed even if it flowed into a central black hole. As shown by Agol (2000), the strong polarization in the radio spectrum of Sgr A* would further constrain the rate of accretion of a magnetically equipartition plasma to be less than about $10^{-9}M_\odot\ yr^{-1}$. In the popular black hole radiatively inefficient accretion flow (Black hole-RIAF) models for Sgr A*, either the estimated Bondi accretion rate is ignored, or it is assumed that there is sufficient angular momentum for the Bondi flow to circularize into a disk from which a jet capable of expelling the excess plasma might be launched. Presumably the hottest part of the disk would be at its inner radius, but this is the part for which the accretion rate must be limited.

On the other hand, while the Bondi flow is expected to be radiatively inefficient for the case of a MECO-Bondi model for Sgr A*, the strong intrinsic magnetic field of the MECO would both disrupt and eject most of the flow before an accretion disk could form. It is well known that stellar magnetic fields can severely inhibit accretion to stellar surfaces (e.g., Toropina et al. 2003). "Magnetic propeller effects" associated with stellar rotation (Romanova et al. 2003, hereafter RTTL03, 2005) can cause additional reductions. Revealing animations of these processes can be viewed

at **http://astrosun2.astro.cornell.edu/us-rus/** . Results displayed in Figure 6 of RTTL03 for the "propeller flow regime" show that there is a converging dense accretion flow to the magnetic poles and a very low density, high speed toroidal equatorial outflow. Significant accretion density variations occur in the polar regions within a few times the object radius. The conical flow into the polar regions provides a plausible compact source of some luminosity from within a few R_g of the central object while the low density outflow would serve as the source of most of the flat spectrum radio luminosity. The matter flowing in on field lines that enter the polar regions can accrete to the surface, but the bulk of the inflowing mass is ejected in the magnetic propeller regime. RTTL03 demonstrated that as little as 2% of the accreting material could reach the central star in their simulations. An even smaller fraction should reach a more compact central MECO with its much stronger magnetic field.

The propeller flow regime occurs if the magnetosphere radius lies between the corotation and light cylinder radii. MECO co-rotation and light cylinder radii are determined by the mass and spin frequency for both GBHC and AGN (RL02, RL03, RL04, RL06), and respectively, have the same range of values given by $\sim 30-100\ Rg$ and $300-1000\ Rg$. As noted by RTTL03, plasma within the magnetosphere corotates with the central object, but only the fraction that penetrates within the corotation radius can accrete to the surface. Figure 7 of RTTL03 shows that beyond the corotation radius, magnetic, centrifugal and pressure gradient forces each exceed the gravitational force and combine to accelerate the equatorial outflow to escape speed.

As shown by RTTL03, the Alfven surface in a Bondi flow has a complex shape. The axial and equatorial magnetospheric radii are unequal. RTTL03 showed good agreement between the equatorial magnetosphere radius of their simulation and the radius calculated from Eq. 13 Table 1, for which the outflow is assumed to occur over about 30% of the 4π solid angle surrounding the dipole. This equatorial radius is determined by equating the energy density of the magnetic field to the kinetic energy density of matter thrown tangentially from the equatorial magnetosphere. The equatorial magnetosphere radius for an accretion rate of $3\times10^{-6}M_{\odot}\ yr^{-1}$ would be $r_m(out) = 3.4\times10^{14}s_1^{-1/5}\ cm \sim 450R_g$ (Table 1 Eq. 13), which is not far inside the light cylinder radius of $3.6 \times 10^{14}/s_1\ cm$. It should be noted that the equatorial magnetic field strength is still $\sim 20\ -\ 40\ \ G$ in the region between magnetosphere and corotation radii, but the kinetic energy density of departing plasma is sufficient to drag the magnetic field lines along with the outflow. In the outflow regions nearer the corotation radius it can be seen in Figure 1 that much of the flow is also loaded onto outward trending portions of the magnetic field lines. The polar magnetosphere radius is determined by the same balance of kinetic energy density and magnetic field energy density along the dipole axis. The basic idea is that when the energy density of the magnetic field exceeds that of the plasma it will control the flow and the plasma will corotate with the field. Since the incoming polar flow merely attaches to field lines having essentially the same direction, no axial magnetospheric shock is expected. The polar axial magnetosphere radius would be $z_m(in) = 1.2 \times 10^{15}\ cm \sim 1800R_g$ (Table 1, Eq. 12). With the corotation radius well within the magnetosphere radius a MECO model for Sgr A* would be in a strong propeller regime.

For a plasma flow to reach a rotating central dipole aligned along the z-axis, it must enter inside the corotation radius. This can occur easily for plasma flowing into the polar regions of the magnetosphere. This part of the flow takes place in a conical portion of

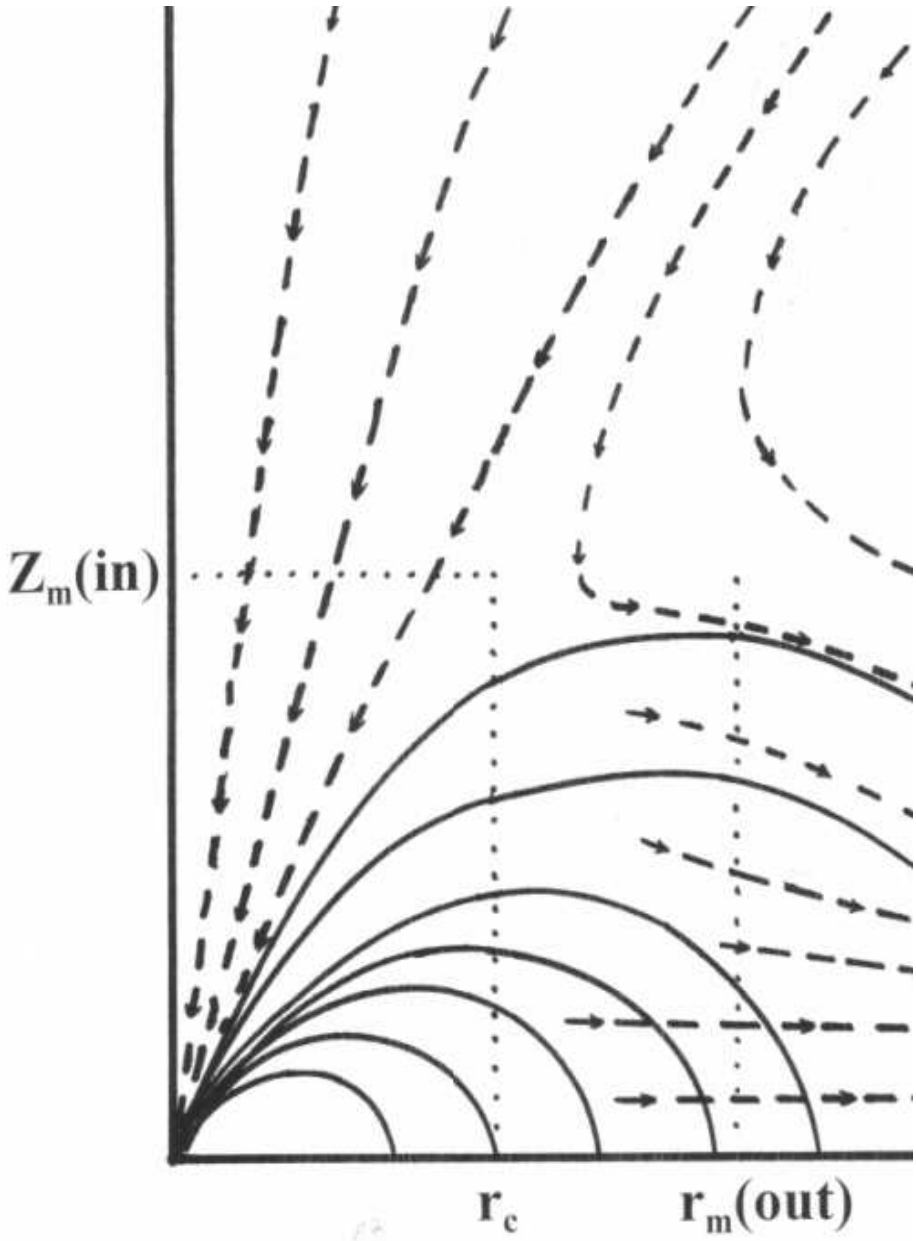

Figure 1: Schematic diagram of accretion flow into a rotating magnetic dipole. Solid lines are magnetic field lines, dashed lines with arrows indicate flow lines. Dotted lines mark corotation and magnetosphere radii. The part of the flow that reaches the axial Alfven surface at $z_m(in)$ and continues to the MECO surface is approximately conical.

a what would be a roughly spherically symmetric flow while the pattern elsewhere is a circulating mix of inflow and outflow. A schematic diagram of the flow is shown in Figure 1. The part of the flow that can reach the central dipole enters at the top and bottom of a cylindrical volume whose flat circular ends have a radius equal to the corotation radius and whose height extends the axial magnetosphere distance, $z_m(in)$ above and below the equatorial plane. The parts of the flow that do not penetrate the corotation radius at $z_m(in)$ are eventually ejected in the low density equatorial outflow. The fraction of a Bondi flow that can reach the central dipole is just the fraction of 4π steradians that is subtended by the corotation circle at distance $z_m(in)$. This fraction is $f = 2\pi r_c^2/(4\pi z_m(in)^2) = r_c^2/(2z_m(in)^2)$. The factor of two in the first numerator is for plasma entering both poles [2]. For $r_c = 4.4 \times 10^{13} s_1^{-2/3}\ cm$ and $z_m(in) = 1.2 \times 10^{15}\ cm$, we find $f = 6.7 \times 10^{-4} s_1^{-4/3}$. For a Bondi rate of $3 \times 10^{-6} M_\odot\ yr^{-1}$ only $\sim 2 \times 10^{-9} s_1^{-4/3} M_\odot yr^{-1} = 1.3 \times 10^{17} s_1^{-4/3}\ gs^{-1}$ would reach the central MECO[3].

The radiation from the accretion flow into a MECO is primarily of cyclotron-synchrotron origin and with frequencies driven by the magnetic field of the MECO. The highest frequencies would be generated where the field strength is greatest. Since plasma in the outflow cannot have gotten closer than the corotation distance to the central MECO, we do not expect it to contribute to the higher energy and frequency NIR spectral components observed for Sgr A*. As described below the NIR, SSC x-rays and some thermal brehmsstrahlung, should be generated in the conical polar inflow. The expanding equatorial outflow would be expected to produce flat spectrum radio emissions similar to those produced by jets. Although some radio emissions would also be produced within the inflow region, the larger amount of outflowing plasma would dominate the radio emissions.

5 ORIGINS OF OBSERVED RADIATIONS

As discussed above, the relatively low accretion rates appropriate for Bondi accretion onto Sgr A* would leave a quiescent MECO surface. From the discussion of Bondi accretion above, we expect spectral characteristics as shown in Figure 2. With this view in mind we can examine some of the plasma conditions and corresponding spectral features of the flow. As described in Appendix E, we have solved the energy equation for spherical flow for application to the axial cones. The characteristics in this part of the flow are determined primarily by conditions at the Bondi radius. This solution clearly does not apply to the more complex flow pattern outside the axial cones. Flow speeds, ion

[2] RTTL03 provided scalable relations for the fraction of Bondi accretion that could reach the central magnetic dipole, however, their simulations used a central object radius of $R_* = 0.0044 R_B \approx 1300 R_g$, which is too large for application to the more compact magnetic MECO. For simulation conditions that would be applicable to Sgr A*, the ratio of corotation radius to Bondi radius would need to be $20\times$ smaller than the smallest ratio of RTTL03. The ratio of magnetic field at the corotation radius to the field at the magnetosphere radius would need to be about $2200\times$ larger than the largest of RTTL03. In view of the comparatively smaller corotation radius and larger magnetic field there we can expect the fraction of the Bondi accretion rate that can reach the central object to be much smaller than the minimal value of $f \sim 0.02$ found in RTTL03.

[3] While this low rate of flow reaching inside the corotation radius would satisfy the proposed constraint imposed by observations of linear polarization (Agol 2000), it is probably irrelevant because the constraint entailed the assumption that the magnetic field was, at most, an equipartition field generated within the flow. The magnetic field strengths shown in Table 3 are so much larger that they would produce strong polarization even for much higher accretion rates.

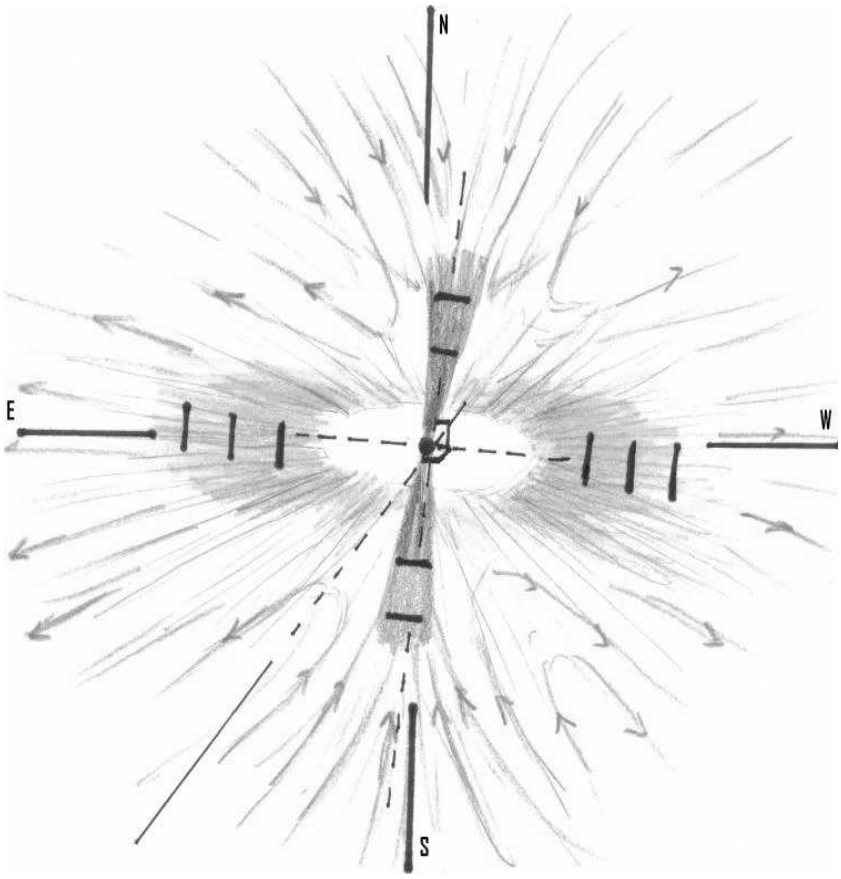

Figure 2: Sketch of Bondi inflow/outflow pattern within the magnetosphere for MECO model of Sgr A*. Most of the radio spectrum to 10^{12} Hz is generated in plasma that departs in an equatorial disk-like outflow. The disk outflows should be both limb brightened and beamed, generally W-E and E-W as seen against the sky plane. NIR would be produced in the generally N-S and S-N axial inflows. Polarization directions marked with dark bars are essentially perpendicular to magnetic field lines. Quiescent x-ray luminosity would be produced throughout the magnetosphere volume. X-ray SSC and thermal brehmsstrahlung radiation would be produced in flares in the axial inflow NIR region. The luminosity of the central MECO, even at its peak luminosity at $3.2\mu m$, is below observational limits.

Table 3: Bondi Flow Plasma, Magnetic and Spectral Parameters

Axial or Radial Eq. Distance (cm)	$T_{9,ion}$ K	$T_{9,e}$ K	v_z $(cm\ s^{-1})$	B_z(G)	$\nu(polar)$	$\nu(out)$	$n(cm^{-3})$	r_L (cm)
$2 \times 10^{17} = R_B$	0.022	0.022					18	
10^{16}	0.23	0.07	1.2×10^8				610	
$10^{15} = z_m(in)$	2.2	0.22	4.9×10^8	1.5	4.1 MHz	$2.04MHz$	1.7×10^4	747
$10^{14} \approx r_m(out, s_1 = 1)$ (equatorial)	22	0.7	1.7×10^9	1460	4.1 GHz	2.04 GHz	5.5×10^5	1.4
$4.4 \times 10^{13} = r_c(s_1 = 1)$	50	1.1	2.6×10^9	1.7×10^4	48 GHz	24 GHz	1.9×10^6	0.08
$2 \times 10^{13} = 30R_g$	109	1.6	3.8×10^9	1.8×10^5	540 GHz		6.1×10^6	0.01
10^{13}	220	2.2	5.4×10^9	1.5×10^6	4×10^{12} Hz		1.7×10^7	2.7×10^{-3}
$2 \times 10^{12} = 3R_g$	1100	5	1.2×10^{10}	1.8×10^8	5.1×10^{14} Hz		1.9×10^8	1.3×10^{-5}

densities and temperatures for the axial flows are shown in Table 3. For a monatomic gas, the flow never becomes supersonic, though it closely approaches sonic speed everywhere in the polar flow within the magnetosphere. The sonic speed is essentially half what the free-fall speed would be. The general character of the flow is such that ion density varies as $n \propto r^{-3/2}$, ion temperature as $T \propto r^{-1}$, flow speed as $v \propto r^{-1/2}$ and electron temperature as $T_e \propto r^{-1/2}$. As described and calculated in Appendix E, the electrons gain the bulk of their energy from collisions with ions but do not thermally equilibrate with them. Electron temperatures, axial magnetic field strength, cyclotron frequencies and Larmor radii are shown in Table 3. The Larmor radii are much larger than the mean particle spacing, $n^{-1/3}$ until $r \sim 30R_g$ and the flow is optically thick until then. The flow is Compton thin throughout.

For a number of reasons, we have limited calculations in Table 3 to $r \geq 3R_g$. First, the energy equation ceases to apply as ion speeds become relativistic and it becomes necessary to distinguish between coordinate speed and physical three-speed in strong gravity. These distinctions do not change the qualitative features obtained by using the energy equation below $30R_g$, which is a little beyond its range of exact applicability. Second, the luminosity generated near $3R_g$ is so refracted gravitationally that it would appear to come from a larger region. Third, the classical dipole expression for the magnetic field begins to need modification as gravitational redshift becomes significant inside $3R_g$ (Appendix B) . Lastly, the gravitational redshift and Lorentz factors reduce the distantly observed cyclotron radiation frequencies by more than the amount that the relativistically enhanced magnetic field increases them. A limiting frequency of a few times 10^{14} Hz is approached near $3R_g$. In effect, the inflow synchrotron spectrum cuts off below the NIR anyway. This interesting limiting frequency is set by the magnitude of the MECO surface magnetic field[4]. In the MECO model, the magnetic field has been constrained to be no larger than that which would produce bound electron-positron pairs on the MECO baryon surface. For this reason it follows that strength of the MECO magnetic moment is not a free parameter, but rather is a result of a quantum electrodynamic stability constraint on the highly red shifted, Eddington limited collapse process of the MECO suface as described by the Einstein-Maxwell equations (see RL06 and Appendix B).

5.1 Spectral Characteristics of the Bondi Flow

The plasma outside the magnetosphere can weakly radiate via thermal brehmsstrahlung and synchrotron processes, but the electrons are generally too cool to produce much

[4]A much weaker magnetic field at $3R_g$ might not produce cyclotron frequencies as high as the NIR. On the other hand, a much stronger field might generate soft x-rays in the axial inflow.

luminosity. Inside the magnetosphere strong, ordered magnetic fields exist and cyclotron emission would be dominant until the accreting electrons become mildly relativistic about at the corotation distance. As shown in Table 3, different cyclotron fundamental frequencies are generated in the polar inflow and the equatorial outflow, but both inflow and outflow can contribute throughout most of the radio frequency range to $\sim 10^{12}\ \ Hz$. The reason for this is that the mean particle spacing, $\propto n^{-1/3}$ is much smaller than the Larmor radius except in parts of the inflow that get inside $\sim 30R_g$. The mean time between collisions, roughly the mean particle spacing divided by the mean electron speed, is $\sim 10^{-12}\ \ s$ until a distance of $\sim 30R_g$ is reached. Hence collision broadening will spread the cyclotron/synchrotron frequency range to about $10^{12}\ \ Hz$ in both inflow and outflow.

For the MECO magnetic moment of $7.3 \times 10^{44}\ G\ \ cm^3$, the strongest magnetic field that electrons in the outflow could encounter would be $\sim 15000\ G$ at the corotation distance on the equatorial plane and the highest cyclotron frequency that they would generate would be 42 GHz, however, as explained, the spectrum produced by electrons that eventually depart in the outflow would be collision broadened to as much as $10^{12}\ \ Hz$. As the outflow continues outward it rapidly becomes less dense, its emissions less collision broadened and generally of lower frequency. Since the lowest cyclotron frequency generated within the inflow and inside the corotation radius would be the $83\ \ GHz$ shown in Table 3, we can say that any lower frequencies would most likely originate in the much larger mass that eventually departs in the equatorial outflow. This picture is consistent with the observation of a flare at $23\ \ GHz$ occurring later than the flare at 43 GHz (Yusef-Zadeh et al. 2008) and thus indicating an outflow with lower frequencies produced further out in the outflow. It would also not be surprising if the major contribution to the earlier corresponding flare observed at $353\ \ GHz$ ($850\mu\ m$) also originated in the outflow, but closer to the corotation boundary distance.

Since the electrons in the outflow cannot get within $\sim 30s_1^{-2/3}R_g$, they can't contribute to frequencies above $\sim 10^{12}\ \ Hz$. Thus we can say that the $10^{12}\ \ Hz$ to NIR range would be generated entirely within the conical axial inflow. In addition, above $10^{12}\ \ Hz$, the Larmor radius becomes smaller than the mean particle spacing. The flow thus becomes optically thin inside $25 - 30R_g$, with fundamental cyclotron frequencies dominating the spectrum without significant collision broadening. This permits us to associate particular frequencies with different positions on the axis ($\nu \propto B \propto z^{-1/3}$). What is even more interesting is the fact that in context of Bondi accretion onto Sgr A*, the differing spectral ranges of the equatorial outflow and the polar inflow predicted by the MECO model for Sgr A* are in agreement with those originally required in the two spectral component model of Sgr A* proposed by Agol (2000).

5.2 Flares and Timing Considerations

Recent measurements (Yusef-Zadeh et al. 2006, 2008) show that x-ray and NIR flares preceded some corresponding flares observed at radio frequencies. However, if NIR originates entirely in the inflow, it would seem that flares in the radio frequencies would also be produced earlier in the inflow by plasma in transit from greater distances. For example, a flare at $10^{12}\ Hz$ (1000 GHz) would be generated in the axial flow field at $\sim 1.4 \times 10^{13}\ \ cm = 25R_g$ compared to a distance of $3 \times 10^{12}\ \ cm = 5.5R_g$ for a NIR flare at $3\mu m$. At an average flow speed of $\sim 7 \times 10^9\ \ cms^{-1}$ (Table 3), the NIR flare should occur approximately 26 minutes later. Assuming that the flares are caused by

variations in the density of material in the Bondi flow, we should actually expect two flares to occur in the radio frequencies. A relatively weak early one should originate in the inflow and a stronger one in the heavier outflow. Differences in flow speed would likely cause them to occur at different times. The inflow is straight down the magnetic field lines at high speed while the plasma in the outflow would be traveling more slowly and changing from inward to outward motion. Its flare would most likely be delayed. As shown in Figure 1 of Yusef-Zadeh et al. (2008) for observations of July 17, 2006 a weak flare at $850\mu m$ (353 GHz) preceded an x-ray flare by about half an hour, which was then followed about 1.4 hours later by another much longer and brighter flare at $850\mu m$. Another observation showed (Yusef-Zadeh et al. 2006, Figure 1b) two NIR flares, each of about one half hour duration and only one flare at $850\mu m$. If the latter is associated with the second NIR flare, then it preceded the NIR by about 38 minutes. No $850\mu m$ measurements are shown beyond the occurrence of the second NIR peak, so we don't know whether or not a larger radio flare followed. Weak radio flares preceding NIR or X-ray flares would be consistent with the MECO inflow. The larger second radio flare occurring after the NIR/x-ray flares would also be expected. While this picture associated with the MECO model is consistent with the flare observations seen in Sgr A*, it is possible that they might also be accommodated by a black hole driven disk-jet RIAF model for Sgr A* in which some radio frequencies would be generated first in the flow into a hot base of an outflowing jet where NIR and x-ray could be produced. Presumably matter of increasing density could flow into the base of a jet and produce some radio flaring before being expelled. Then there could also be another set of radio flares frequencies produced later further up a jet outflow.

Considering the weakness of the observed $850\mu m$ flares that preceded the observed NIR and X-ray flares, it is conceivable that weak NIR/x-ray flares could be observed without noticeable earlier flaring at radio frequencies in the Bondi inflow. Because of the slower flows near the corotation radius in a magnetic propeller outflow, a NIR/x-ray flare without much of a preceding radio flare could still be produced before any radio flares, thus giving a progression of flares that might all be thought to occur in an outflow. Lastly, depending on the size and location of clumps of matter in the incoming Bondi flow, it would be possible for enhanced density to only occur in the outflow portion and produce radio flaring without producing either x-ray or NIR flares. Although these considerations make it seem plausible that we could have combinations of NIR/x-ray or radio flares without always having both, it seems likely that the strongest NIR/x-ray flares would always be associated with both preceding and trailing radio flares in the MECO model.

5.3 Luminosities

As shown in Appendix E, (Eq. 42) the luminosity produced in the axial inflows to distance z from the MECO is approximately

$$L = 6.4 \times 10^{40} s_1^{-4/3} z^{-1/2} \quad ergs^{-1} \tag{2}$$

For $z = 3R_g = 2 \times 10^{12}\ cm$, and $s_1 = 1$ this yields $L = 4.5 \times 10^{34}$ erg s^{-1}, which is lower than observed by only about a factor of 3.8. The coulomb scattering cross-section that enters the development of Eq. 2 is probably not known to any better accuracy. To $30R_g$ and 540 GHZ, the calculated luminosity in the polar flow would be 1.4×10^{34} erg s^{-1}. For comparison, the spectrum reported by An et al. (2005) shows a luminosity of

1.7×10^{35} erg s^{-1} to a frequency of 540 GHz. Thus the discrepancy between these results occurs primarily in the lower frequencies. The flux at 10^{12} Hz consistent with Eq. 2 is about one order of magnitude below the observed radio spectral trend. This should be expected because most of the radio spectrum would be generated in the magnetic propeller driven outflow.

At frequencies above about 10^{12} Hz, the axial flow is optically thin and dominated by cyclotron fundamental frequencies that can be associated with position in the dipole magnetic field; i.e., $\nu \propto B \propto z^{-3}$. Thus inside $30R_g$, it is also shown in Appendix E that luminosity varies with frequency along the axial flows such that (Appendix E Eq. 43)

$$dL = 2.7 \times 10^{31} s_1^{-4/3} \nu^{-5/6} d\nu \qquad ergs^{-1} \tag{3}$$

Thus the spectral index in the optically thin IR/NIR would be $-5/6$ for the conical inflow model. The average of four measurements reported in BN06 in the NIR wavelength range from $1.6-4.8\mu m$ is 4.7 mJy. Using a distance to Sgr A* of 8 kpc, the average flux calculated here from Eq. 3 for the same four wavelengths is $0.74 s_1^{-4/3}$ mJy. Again, this result could likely be improved with a better Coulomb cross-section, but the spectral index is an important result that depends only upon electron temperature varying as $\sqrt{z}$. The variability shown by NIR measurements at the position of Sgr A* strongly suggests that the NIR spectrum originates in a variable accretion flow that is consistent with the MECO model. While the flux calculated here is somewhat larger than the lowest flux used in BN06 to constrain an accretion rate to an assumed hard surface, it should be remembered that variability in the accretion flow would produce opportunities to observe both higher and lower luminosities.

In addition to sensitivity to the electron temperature, the luminosity generated in the inflow depends on the MECO spin rate which then determines the size of the corotation radius ($\propto \nu_s^{-2/3}$) and hence the fraction of the Bondi flow that can reach the central MECO is proportional to $s_1^{-4/3}$. Exact agreement between calculated and average observed NIR fluxes could be achieved with the choice $s_1 = 0.25$. While such an empirical adjustment of the spin parameter s_1 associated with the MECO in Sgr A* is within reason, the value of s_1 determined in this manner is subject to the caveat that a large factor of uncertainty still remains in the relevant value of the Coulomb collsion cross-section.

For an optically thick slice in the inflow normal to the polar axis and at frequencies below 540 GHz, the cyclotron spectrum would produce luminosity from a region of thickness dz that would be proportional to $2\nu^2 kT_e/c^2$ times lateral surface area $2\pi r_c z/z_m dz$. The correlation of frequencies with position, z, in the inflow is surely weaker in the broad radio spectral band, but if we still associate z with frequency as $z \propto \nu^{-1/3}$, the luminosity from the band would then be proportional to $\nu^{2-1/3-4/3} d\nu$, hence the spectral index for the optically thick band between 51 GHz and 560 GHz would be $+1/3$, compared to the reported 0.43 (An et al. 2005). On the other hand, if viewed looking parallel to the equatorial plane, the luminosity in the outflow could be calculated in the same way in a series of slices of thickness dz with outflow radius proportional to $\nu^{-1/3}$ ($\propto B^{-1/3}$) to obtain the same spectral index. Both radio and NIR spectral indexes are sensitive to the shape of the conical inflow pattern. Dipole magnetic field lines have some curvature that would slightly widen the cone at the top. If the "cone" radius were proportional to z^b with $b > 1$, it would increase the overall luminosity and spectral index calculated for the NIR and decrease the spectral index in the optically thick region below the spec-

tral peak. This suggests that some refinements of our MECO-Bondi model might be expected to produce closer agreement with observations but that is a task for another time.

Electrons become mildly relativistic with Lorentz factors of $\gamma_e \sim 2-3$ for small z. Some x-ray emission would arise from Compton scattering within $\sim 30R_g$ in the polar inflow. Electron densities are also large enough in this region to produce some thermal brehmsstrahlung. The calculation of synchrotron self-compton (SSC) contribution can be started by differentiation of Eq. 2 to obtain the luminosity contribution from axial thickness dz as $|dL| = 3 \times 10^{40} z^{-3/2} dz = (dN_\nu/dt)E_\nu$, where dN_ν/dt is the rate of production of synchrotron photons of average energy E_ν within dz. In passing through distance $r = zr_c/z_m$, on average, these photons will experience $n_e \sigma_T r$ collisions, where n_e is the electron density and σ_T the Thompson cross-section. The average energy gained per collision would be $2(\gamma_e+1)E_\nu(kT_e/m_e c^2)$. Substituting for n_e, T_e and r as a function of z, and integrating over z, gives the x-ray self-synchrotron luminosity as

$$L_{SSC} = 5.4 \times 10^{48} z^{-3/2} \qquad ergs^{-1} \tag{4}$$

which provides about 6×10^{28} erg s^{-1} to $3R_g$.

For a gaunt factor of ~ 5 for small z, thermal brehmsstrahlung contributions can be calculated similarly. The emissivity obtained is $6.2 \times 10^9 z^{-2.75}$ $erg\ s^{-1}\ cm^{-3}\ Hz^{-1}$. Integration over the axial cone volume and all frequencies yields a thermal (primarily x-ray) luminosity of

$$L_t = 4 \times 10^{33} z^{-1/4} \qquad ergs^{-1} \tag{5}$$

This provides another $\sim 3.4 \times 10^{30}$ erg s^{-1} to $3R_g$.

Though both calculated x-ray luminosities might be increased somewhat by considering a flared "cone", their combined contributions should still fall well below the 2.4×10^{33} erg s^{-1} observed in the 0.5 - 7 keV band (Baganoff et al. 2003). Nevertheless, both depend on the square of electron density which could enhance their contributions to the luminosity in flares relative to synchrotron luminosity. These x-ray luminosity variations in flares would be strongly correlated with the NIR synchrotron luminosity variations and essentially without time delays since both originate in the same population of electrons.

A substantial fraction of the quiescent x-ray luminosity appears to come from a spatially extended source (Baganoff et al. 2003). There is a considerable volume in the MECO magnetosphere in which temperatures and densities would be high enough to produce thermal x-rays. Within the rough bounds of the magnetosphere outside the corotation radius there is a volume of $2\pi r_m(out)^2 z_m(in) \sim 3 \times 10^{44}$ cm^3. Using 10^{14} cm as an average radius in the Bondi flow, we estimate the corresponding electron temperature to be 10^9 K and the electron density to be 10^6 cm^{-3}. For these parameters, a gaunt factor of 3 and the 1.6×10^{18} Hz bandwidth from 0.5 - 7 keV, we find an average thermal brehmsstrahlung emission rate of 10^{-11} $ergs^{-1}cm^{-3}$. Multiplying by the magnetosphere volume, we obtain $\sim 3 \times 10^{33}$ erg s^{-1}, which is reasonably close to the observed quiescent x-ray luminosity of Sgr A*.

The axial inflows constitute such a small fraction of the Bondi accretion rate that their contributions to the spectrum below 48 GHZ are much smaller than the radiation from the much larger outflow. We don't know how much the outflows might contribute in harmonic frequencies above 24 GHz, but since the luminosity calculated for the axial flow did not account for the observed luminosity or flux to a frequency of 540 GHz, there

is a significant contribution from the outflow that has not been considered. Accurately quantifying the radio luminosity will require knowledge of the plasma and magnetic field distributions, as previously mentioned. All that we can do here is set an upper limit on what might be produced in the outflow. For an accretion rate of $2 \times 10^{20}\ gs^{-1}$, electrons would flow outward at a rate of $1.2 \times 10^{44}\ s^{-1}$. If they each had the energy they could extract from the protons while reaching the corotation radius, there would be about 2×10^{37} erg s^{-1} available for radiation. The actual radiation rate would probably be much smaller as few of the electrons that would flow out would reach such small distances from the MECO. In this regard, in reaching a steady state, the magnetic propeller eventually must drive the outflow beyond the Bondi radius, cutting off a large fraction of the flow into the Bondi sphere and eventually producing a large torus where the outflow stops beyond the Bondi radius[5]. A luminosity of a few times 10^{36} erg s^{-1} would seem to be entirely reasonable. Another way of looking at this is to consider that approximately $2 \times 10^{-9} M_\odot\ yr^{-1}$ is swallowed by the MECO. We have accounted for the luminosity that it produces in the axial inflow. Unlike the mass that escapes in the outflow, the amount of energy that it could give up in reaching the corotation radius would not be needed for its escape. The luminosity that it could produce in reaching the corotation radius would be about $L = GM\dot{m}_\infty/2r_c \sim 10^{36} s_1^{2/3}$ erg s^{-1}.

5.4 Polarization

The MECO-Bondi flow pattern has two major regions of strong, ordered magnetic fields, with the strongest fields along the polar axis. With the NIR generated within the the polar inflow, its linear polarization direction would be essentially perpendicular to the axis. The equatorial outflow would produce magnetic field lines that spiral outward along the outflow. These field lines would be perpendicular to the magnetic polar axis and there are several possibilities for what might be observed, depending on the orientation of the magnetic axis and equatorial plane relative to an observer. Yusef-Zadeh et al. (2006) showed some evidence of outflow from Sgr A*. The apparent flow was in a generally WSW direction from Sgr A*. Proper motion studies have provided confirmation (Muzic et al., 2007) of a general, uncollimated outflow. GRAVITY, a recently proposed high resolution interferometric imaging system (Eisenhauer 2008), should be capable of revealing the nature of the plasma flows in the vicinity of Sgr A* in unprecedented detail. If what has been observed at radio frequencies would be a view into the MECO-Bondi equatorial outflow, momentarily neglecting beaming, we would see the limb brightened regions of the outflow extending WSW (and ENE) against the plane of the sky, with magnetic field lines spiraling out along the flow. Linear polarizations from the outflow would then be generally perpendicular to the magnetic field lines and in the SSE-NNW direction. A sketch of the way this might appear is shown in Figure 2. This radio polarization has been observed at 230 GHz (Bower et al. 2003) and clearly displayed, aligned perpendicular to the WSW-ENE direction of the outflow. (See Fig. 2.1, http://www.cfa.harvard.edu/sma/newsletter/
smaNews_21Dec2006.pdf). Weaker polarization would be produced further out in the

[5]Note that the simulations of RTTL03 never reached this steady state. Cutting off a substantial fraction of the accretion flow could have a significant effect on the inflow rate and thus affect the luminosity generated in the outflow beyond the corotation radius, but it probably would not greatly affect our estimated luminosity in the polar flow, which depends primarily on the spherical flow pattern in the polar regions and the asymptotic values of density, n_∞ and temperature T_∞ at the Bondi radius.

flow where the field is weaker and fundamental cyclotron frequencies would be lower.

In addition to the polarization direction at radio frequencies matching expectations for an outflow, strong polarization has been observed in the NIR with a direction roughly 90 degrees (ENE) different from that seen at radio frequencies (Eckart et al. 2008). As noted, this is consistent with the polarization that should be seen perpendicular to the field lines in the inflow if viewed at high inclination to the inflow axis. A view with this orientation would be a view fairly directly into the equatorial outflow. Because of the dipole nature of the MECO magnetic field, a view directly into the equatorial plane would have outgoing magnetic field lines on one side of the the plane and ingoing field lines on the other. Outflowing electrons would produce left circular polarization from outflow on one side of the equatorial plane and right circular polarization from the other. There would be a net circular polarization only if viewed at some inclination to the outflow equatorial plane. This could occur while still having a large inclination relative to the inflow axis. Electrons spiraling outward on field lines directed toward us would produce a (negative) left circular polarization. The circular polarization ($\sim 1\%$) of Sgr A* (Bower 2000) is unusually strong for an AGN. It seems unlikely that it would originate in a depolarizing medium. While it exhibits short-term variability, it has maintained a stable (negative) sense for over 25 years. In this context it is important to note that the observation of stable directions, with some variability in flares, for both linear and circular polarizations are unique observable features of the MECO model for Sgr A*. All of these properties are determined by the strength of the intrinsic magnetic field of the MECO within the center of Sgr A*. s

5.5 Image Appearances

The observed polarizations are consistent with a view close to the equatorial plane of the outflow and across the axial inflow as shown in Figure 2. For this orientation we should see an increasingly wide outflow zone at longer radio wavelengths. Inside any surface of constant magnetic field strength cutting through the outflow, we would expect optically thick cyclotron radiant flux of $j_\nu = 2\nu^2 kT_e/c^2$ to be generated. The apparent size of its limb brightened photosphere image in the equatorial outflow would be roughly[6] proportional to $\nu^{-2} \propto \lambda^2$ and ellipsoidal as has been observed (Bower et al. 2004). The major axis of the ellipsoid is apparently aligned with the direction of outflow (Muzic et al. 2007, Yusef-Zadeh et al. 2006, Bower et al. 2004) and perpendicular to the radio polarization direction (Bower et al. 2003). These observations are consistent with our prediction that the apparent size and ellipsoidal shape of the radio images of Sgr A* are due to the equatorial outflow from a MECO in the center of Sgr A*.

As observed at 230 GHz (Doeleman et al. 2008) the luminosity of Sgr A* is consistent with a spherical gaussian source of $37\mu as$ radius at half maximum luminosity, however, the observations have not yielded a reconstructed image. They are also consistent with an annular source with inner radius of $35\mu as$ and outer radius of $80\mu as$. For a MECO, a frequency of 230 GHz is likely to be produced predominately within a region fairly near the corotation radius in the outflow. If the entire outflow were uniformly bright, then the image size for the MECO would be about $r_c \sim 350\mu as$, however, with plasma being thrown off tangentially, the radiation from one side would be strongly beamed and radiation from the other side suppressed. It is possible that the spin rate parameter

[6]The limb brightened region viewed would not be a surface of constant magnetic field and would not correspond to a size exactly proportional to λ^2 throughout.

s_1 for the MECO-Bondi model might need to be increased to reduce the size of the model emission region, however, that would also affect the amount of polar inflow and luminosities in the NIR. Further radio observations are needed first and these need to be carefully indexed with the NIR images on the sky plane to determine the spatial distributions of both emissions.

Scattering theory predicts image sizes proportional to λ^2. The image sizes (Bower et al. 2004, Shen et al. 2005) have been interpreted only as scattering features superimposed on a compact object even though the major axis of the observed ellipsoids is twice the length of the minor axis. The galactic center scattering screen is two to three orders of magnitude greater than what is seen in NGC6334B, the next most scattered source (Bower et al. 2004). A heavy screen would be expected for the base of the MECO outflow where its highest radio frequencies would be generated. The earlier claimed detection of an intrinsic size of $48R_g$ for Sgr A* (Shen et al. 2005) rests on apparent deviations from the scattering theory with its wavelength exponent of 2, but for the cyclotron-synchrotron radiations considered here the exponent and deviations at distances inside the corotation radius could arise in a different way. Only much less luminous radio emissions should be generated in the inflow at wavelengths below about 0.3 mm (10^{12} Hz). Eq. 43 (Appendix E) gives an expected flux of 0.25 Jy for this wavelength and a distance of 8.4 kpc to Sgr A*.

As shown above, the surface emissions from a MECO model for Sgr A* would peak well below detection limits at $3.2\mu m$. At wavelengths differing by a factor of even two from the thermal peak a MECO would be as dark as a black hole (see Appendix A - C). Since we identify the 10^{12} Hz to NIR spectrum as originating in concentrated axial flows into the magnetic poles, we would expect image sizes at optically thin wavelengths to no longer be proportional to λ^2 and to be elongated along the inflow axis rather than the equatorial plane. In the optically thin flow, axial distance from the MECO should be correlated with frequency as $z \propto \nu^{-1/3} \propto \lambda^{1/3}$. Hence on the basis of the MECO model for Sgr A* we are led to the prediction that, if viewed at high inclination to the polar axis, there would be two axial lobes, beginning at about $25R_g$ and extending ever closer to a central dark source at shorter wavelengths. Depending on the inclination there might be significant Doppler boosting in the lobe with flow components directed more toward us, however at these radial distances there would not be a uniform background of sub-mm to NIR radiation against which a very dark shadow of the MECO could be viewed. There would be such a background only for wavelengths that originated inside $\sim 5R_g$ and were extremely refracted gravitationally. These wavelengths would necessarily be in the NIR.

For black hole models, there is still a vigorous debate over whether the emission of Sgr A* is produced predominantly by a hot accretion disk or from an energetic outflow (Fish et al. 2009). The constraints provided by the multiwavelength spectrum, variability and polarization of Sgr A* do not yet conclusively establish the nature of the emission region. Nevertheless, the MECO-Bondi model presented here can be compared to some extent with the radiatively inefficient accretion flow (RIAF) into a black hole[7] (Yuan, Quataert

[7]While the expected appearances of MECO and RIAF models are sufficiently different to eventually be clearly observed, there are some theoretical objections that can be raised about the RIAF model. 1) The RIAF model is aesthetically unappealing since it appears to be based on a collection of ad hoc assumptions which have been added onto the original ADAF model in order to allow it to be able to explain the Sgr A* observations. 2) One has to assume a consistent long term angular momentum within the Bondi inflow into Sgr A* in order to get the flow to circularize and form an accretion disk.

& Narayan 2003). To produce the observed polarization of the optically thick radio emission, the internally generated magnetic field of the RIAF would need to be oriented generally E-W. This might occur in two different ways. (a) If the RIAF magnetic field responsible for the polarization were toroidal within the thick RIAF disk, the RIAF disk would need to be seen nearly edge-on in order to have a consistent magnetic field direction as seen from our side. There would only be one direction of flow observed, either E-W or W-E, in the radio. Accordingly, a suitable radio interferometric array analogous to the proposed NIR GRAVITY array (Eisenhauer et al. 2008) might be able to distinguish a RIAF from a MECO outflow. But in the NIR, the RIAF flow might show no preferential direction as observed with the GRAVITY array because both near and far sides could be seen at once if sufficiently optically thin. The NIR, which would be produced closer to the central black hole is optically thin and would be produced in part by non-thermal electrons. It is the power-law distribution of non-thermal electron energies in the optically thin part of the flow that would produce the orthogonal polarization of the NIR (Agol 2000). (b) If the RIAF magnetic field were poloidal; i.e., with field lines emerging perpendicular to the disk, then the disk would need to be oriented generally N-S, but again seen nearly edge on. Again the flow would appear to be unidirectional. The orthogonal polarization of the NIR would then arise in the same way as before. Thus with either orientation, both polarizations would originate in the geometrically thick disk of the RIAF and it should not look the same as the two zone flow of the MECO-Bondi model shown in Figure 2.

It is clear that the accretion rate in a RIAF must be of order $10^{-9} M_{\odot}\ yr^{-1}$, and far below the Bondi rate of $3 \times 10^{-6} M_{\odot}\ yr^{-1}$ in order to produce the observed strong linear polarization within the flow. Exactly how the RIAF might accomplish this is unknown. It has been suggested that the disk evaporates in a wind or that a jet outflow occurs. For a jet outflow to be consistent with observations (Yusef-Zadeh et al. 2006, Muzic et al. 2007, Bower 2003) the RIAF disk would need to be aligned generally N-S with a generally E-W jet. Though this would give more of the appearance of Figure 2, a jet would be an actual collimated outflow rather than just a limb brightened and beamed region of a toroidal outflow and the flow in the RIAF disk would still be unidirectional rather than into the central region from both above and below as in the flow into the poles of a MECO. The GRAVITY array should be able to distinguish these possibilities. Ironically, if inflows were observed to disappear into an unseen dark object from both above and below, it could be mistaken for the flow into a black hole event horizon, but some explanation would then be required for an equatorial outflow which ought to also

3) Assuming that such a Black Hole RIAF accretion disk can be formed by the Bondi inflow, it is then required that most of this disk must "evaporate" and ultimately escape as a wind or be ejected in a jet outflow. If the latter, the jet must be formed at considerable distance, probably beyond $20 - 30 R_g$, by means not presently known. There would be too much luminosity generated by a flow that continued into a Kerr-metric ergospheric jet. Simply ignoring the Bondi accretion rate is not a reasonable option. 4) If the flow is hot enough to produce the quiescent soft x-rays over an extended region, why does it not produce more and harder luminosity in the RIAF part of the flow 5) While it is clear that a source of non-thermal electrons must exist within the black hole RIAF model there still remains an unsolved problem about the source of their energy. Clearly these non-thermal electrons cannot have been accelerated by magnetic reconnection processes because if that were the case then the black hole RIAF would be too bright in the NIR to fit the Sgr A* observations. In spite of these problems, a black hole RIAF with a suitably low assumed disk accretion rate can be used to account for most of the spectral distribution that has been observed, provided that it would be allowed to produce some radio emission in the disk as well as the jet. This is necessary in order to account for the observed timing of NIR/x-ray flares with both preceding and trailing radio flares.

be observed

6 Summary

We have shown that the MECO-Bondi model for Sgr A* can account for the lack of observed surface luminosity from Sgr A* and that a spectrum of approximately correct luminosity and spectral indexes will be produced in the inflow-outflow zones of the Bondi accretion flow into the magnetic field of the MECO. Future calculations leading to more details about the spatial and spectral energy distributions will require more knowledge about the global distributions of electron density and magnetic fields involved. The equatorial outflow would produce optically thick cyclotron radiation with small positive spectral index at frequencies below $\sim 1000\ GHz$. The axial inflow would produce steeply declining (negative index) optically thin NIR emissions as well as some correlated x-ray SSC and brehmsstrahlung emissions that could be observed in flares caused by high density clumps in the inflow. We have shown that timing of flares in radio/NIR/x-ray bands is consistent with the MECO-Bondi model, with some weak sub-mm flaring preceding the strongest NIR and SSC x-ray flares which are then followed by stronger delayed sub-mm and radio flare emissions.

The part of the Bondi flow that eventually departs in the equatorial outflow would produce radio emissions, possibly to frequencies as high as $\sim 1000\ GHz$, and including nearly everything below $\sim 50\ GHz$. The bulk of the quiescent x-ray luminosity would be thermally generated within the magnetosphere in a mixed inflow/outflow pattern of $10^{14-15}\ cm$ size. We have shown that the low bolometric luminosity of Sgr A* can be reconciled with an expected Bondi accretion rate in a completely natural way. The MECO magnetic propeller mechanism is a robust, stable physical mechanism for reducing the Bondi accretion rate to levels compatible with the low luminosity of Sgr A*. The only parameters that have been necessary for these calculations are the ion density and sound speed at the Bondi radius, mass, magnetic moment and spin. The first three of these have been taken from work reported by others. The intrinsic magnetic moment of a MECO is an inherent, mass dependent feature which is generated by the effects of the quantum electrodynamic stablility conditions that are required by the Einstein-Maxwell equations that describe the highly red shifted Eddington limited MECO collapse process (RL06 and Appendix B). Its magnitude sets a natural high frequency limit for the synchrotron emissions in the axial inflow. Our empirical estimate of spin of the MECO in Sgr A* has been retained from our previous work that accounted for the radio/x-ray luminosity correlations and spectral state switches for AGN and GBHC (RL04) and the microlensed images of the quasar Q0957+561 and Q2237 (Schild, Leiter & Robertson 2006).

The highly red shifted Eddington limited, general relativistic MECO model for Sgr A* lacks an event horizon or a "hard surface". It contains an intrinsic magnetic moment that can interact with the Bondi accretion environment of Sgr A*. The intrinsic MECO magnetic moment automatically produces the ordered magnetic fields necessary to account for the observed strong linear polarization. In the MECO-Bondi inflow-outflow model for Sgr A* described here, there are regions of differing magnetic field strength and orientation, strong density variations and both inflows and outflows. We have shown that there are places of origin in this flow for all of the spectral, spatial, polarization and timing features that have so far been observed for Sgr A*. The patterns of inflow and

outflow differ from those expected of black hole models and should be observable by the proposed GRAVITY array (Eisenhauer et al. 2008). On the basis of the MECO-Bondi model for Sgr A* we predict that high resolution images in radio frequencies should be produced in the outflow zone, while high resolution images in NIR and shorter wavelengths should be elongated along an orthogonal polar axis. Since the emissions in these shorter wavelengths are confined to the narrow axial inflow region, there would be no uniform background to provide a silhouette image of a dark MECO except for strong gravitational refraction effects on NIR frequencies generated inside $\sim 5R_g$. Everything inside $\sim 25R_g$ should just be dark in the radio frequencies.

The qualitative consistency of the MECO-Bondi model provides added incentive for doing additional simulations which, in order to succeed, will require substantial computational facilities and expertise. Calculations of the global magnetic field and density distributions will be necessary first steps before synchrotron emissions in the outflow can be calculated. In order to add spectral details, smaller calculation grids close to the central dipole and consideration of light paths in strong field gravity will be required and could be challenging, even for the original US-Russia supercomputer collaboration that produced the work of RTTL03. Calculations extending into the region near the photon sphere ought to be able to provide spectral and image details that could be compared with the increasingly high resolution images of Sgr A*. Further corroboration of the MECO-Bondi model for Sgr A* could be found if future observations eventually reveal NIR lobes for accretion flow into the magnetic polar regions, though they would likely be smeared into ellipsoids by gravitational refraction. A pattern of expected polarizations of radiation should also be computed. The MECO parameters for spin and magnetic moment used here provide a place to start, but for best comparisons these parameters, as well as the Bondi flow parameters should be varied. Rather detailed calculations of what might be seen for different axis orientations will also be necessary. It is our hope that the present paper will provide motivation for this additional work to be joined by others.

References

Abramowicz, M., Kluzniak, W. & Lasota, J-P, (2002) No Proof of the Black Hole Event Horizon, Astronomy & Astrophysics, 396, L31

Agol, E. (2000) Sgr A* Polarization: No ADAF, Low Accretion Rate and Non-Thermal Synchrotron Emissions, Astrophysical Journal Letters, 538, L121

An, T., et al. (2005), Simultaneous Multi-Wavelength Observations of Sgr A*, Astrophysical Journal, 634,49

Baganoff, F., et al. (2003) Chandra X-ray Spectroscopic Imaging of Sagittarius A* and the Central Parsec of the Galaxy, Astrophysical Journal, 591, 891

Baumgarte, T. & Shapiro, S. (2003) Collapse of a Magnetized Star to a Black Hole, Astrophysical Journal, 585, 930

Bower, G. (2000) Polarization in Sgr A*, GCNEWS 11, 4

Bower, G., et al. (2004) Detection of the Intrinsic Size of Sagittarius A* Through Closure Amplitude Imaging, Science, 304, 704

Broderick, A., & Narayan, R. (2006) On the Nature of the Compact Dark Mass at the Galactic Center, Astrophysical Journal Letters, 638, L21 BN06

Broderick, A., Loeb, A., & Narayan, R. (2009) The Event Horizon of Sagittarius A*, Astrophysical Journal, 701, 1357 BLN09

Broderick, A, Fish, V., Doeleman, S. & Loeb, A. (2009) Estimating the Parameters of Sagittarius A*'s Accretion Flow Via VLBI, Astrophysical Journal 697, 45-54

Campana, S. et al. (2002) The Quiescent X-Ray Emission of Three Transient X-Ray Pulsars, Astrophysical Journal 580, 389

Campana, S. et al. (1998) The Neutron Stars of Soft X-Ray Transients, Astronomy & Astrophysics Review 8, 279

Cavaliere, A. & Morrison, P. (1980) Extreme Nonthermal Radiation From Active Galactic Nuclei, Astrophysical Journal Letters 238, L63

Corbel, S., Fender, R.P., Tzioumis, A.K., Nowak, M.A., McIntyre, V., Durouchoux, P.,Sood, R. (2000) Coupling of the X-ray and Radio Emissions in the Black Hole Candidate and Compact Jet Source GX339-4, Astronomy & Astrophysics 359, 251

Corbel, S., Nowak, M.A., Fender, R.P., Tzioumis, A.K. Markoff, S. (2003) Radio/X-ray Correlation in the Low/Hard State of GX339-4, Astronomy & Astrophysics 400, 1007

Doeleman, S. et al. (2008) Event Horizon Scale Structure in the Supermassive Black Hole Candidate at the Galactic Centre, Nature, 455, 78

Eckart, A. et al. (2008) Polarized NIR and X-Ray Flares From Sgr A*, Astronomy & Astrophysics, 479,3, 625-639 /astro-ph0712.3165

Eisenhauer, F., et al. (2008) GRAVITY: Getting to the Event Horizon of Sgr A*, Proceedings SPIE 7013, 70132A, Astronomical Instruments, 22-28 June, Marseille, France, astro-ph/0808.0063

Falcke, H., Körding, E., Markoff, S. (2004) A Scheme to Unify Low Power Accreting Black Holes - Jet Dominated Accretion Flows and the Radio/X-ray Correlation, Astronomy & Astrophysics, 414, 895

Falcke, H., & Markoff, S. (2000) The Jet Model For Sgr A*: Radio and X-ray Spectrum, Astronomy & Astrophysics 362, 113

Fish, V., Broderick, A., Doeleman, S., & Loeb, A. (2009) Using Millimeter VLBI to Constrain RIAF Models of Sagittarius A*, Astrophysical Journal Letters 692, L14-L18

Ghez, A. et al. (2005), Stellar Orbits Around the Galactic Center Black Hole, Astrophysical Journal 620, 744

Ghez A. et al. (2008), Measuring Distance and Properties of the Milky Way's Central Supermassive Black Hole With Stellar Orbits, Astrophysical Journal 689, 1044

Gallo, E., Fender, R., Pooley, G. (2003) A Universal Radio/X-Ray Correlation in Low/Hard State Black Hole Binaries, Monthly Notices of the Royal Astronomical Society, 344, 60

Gliozzi, M., Bodo, G. & Ghisellini, G. (1999) The Bulk Kinetic Power of the Jets of GRS 1915+105, Monthly Notices of the Royal Astronomical Society, 303, L37

Gupta, A., Mishra, A., Mishra, H., & Prasanna, A.R. (1998) Rotating Compact Objects With Magnetic Fields, Classical and Quantum Gravity, 15, 3131

Heinz, S., Sunyaev, R. (2003) The Non-Linear Dependence of Flux on Black Hole Mass and Accretion Rate in Core Dominated Jets, Monthly Notices of the Royal Astronomical Society 343, L59

Harding, A. (2003) Physical Processes in Strong Magnetic Fields of Neutron Stars, Invited talk at Pulsars, AXPs and SGRs Observed with BeppoSAX and Other Observatories, Marsala, Sicily, Sept. 2002 astro-ph/0304120.

Ilarianov, A. & Sunyaev, R. (1975) Why the Number of Galactic X-Ray Stars is So Small?, Astronomy & Astrophysics, 39, 185

Kippenhahn, R. & Weigert, A. (1990) 'Stellar Structure and Evolution' Springer-Verlag, Berlin Heidelberg New York

Landau, L. & Lifshitz, E. (1958) 'Statistical Physics', Pergamon Press LTD, London

Leiter, D., & Robertson, S. (2003) Does the Principle of Equivalence Prevent Trapped Surfaces From Being Formed in the General Relativistic Collapse Process?, Foundations of Physics Letters, 16, 143

Maccarone, T., Gallo, E., Fender, R. (2003) The Connection Between Radio Quiet AGN and the High/Soft State of X-Ray Binaries, Monthly Notices of the Royal Astronomical Society 345, L19

Markoff, S., Falcke H., & Fender, R. (2001) A Jet Model for the Broadband Spectrum of XTE J1118+480: Synchrotron Emission From Radio to X-Rays in the Low/Hard Spectral States, Astronomy & Astrophysics Letters, 372, 25

Markoff, S., Nowak, M., Corbel, S., Fender, R., Falcke, H. (2003) Modeling the X-Ray Contribution of X-Ray Binary Jets, New Astronomy Reviews, 47, 491

McClintock, J., Narayan, R., and Rybicki, G. (2004) On the Lack of Thermal Emission From the Quiescent Black Hole XTE J1118+480: Evidence For the Event Horizon, Astrophysical Journal, 615, 402

Mitra, A., & Glendenning, N. (2010) Likely Formation of General Relativistic Radiation Pressure Supported Stars or "Eternally Collapsing Objects", Monthly Notices of the Royal Astronomical Society, in press, arXiv:1003.3518 [astro-ph.HE]

Mitra, A. (2006a) Sources of Stellar Energy, Einstein-Eddington Timescale of Gravitational Contraction and Eternally Collapsing Objects, New Astronomy, 12, 146-160

Mitra, A. (2006b) Radiation Supported Stars in Einstein Gravity: Eternally Collapsing Objects, Monthly Notices of the Royal Astronomical Society 369, 492

Mitra, A. (2006c) Why Gravitational Contraction Must be Accompanied by Emission of Radiation Both in Newtonian and Einstein Gravity, Physical Review D, 74, 034010

Muzic, K., et al. (2007) First Proper Motions of Thin Dust Filaments At the Galactic Center, Proceedings of the International Astronomical Union, 2, 415

Rezzola, L., Ahmedov, B., Miller, J. (2001) Stationary Electromagnetic Fields of a Slowly Rotating Magnetized Neutron Star in General Relativity, Foundations of Physics, 31, 1051

Robertson, S. & Leiter, D. (2002) Evidence For Intrinsic Magnetic Moments in Black Hole Candidates, Astrophysical Journal, 565, 447 RL02

Robertson, S., Leiter, D. (2003) On Intrinsic Magnetic Moments in Black Hole Candidates, Astrophysical Journal Letters, 596, L203 RL03

Robertson, S., Leiter, D. (2004) On the Origin of the Radio/X-ray Luminosity Correlation in Black Hole Candidates, Monthly Notices of the Royal Astronomical Society, 350, 1391 RL04

Robertson, S., and Leiter, D. (2006) 'The Magnetospheric Eternally Collapsing Object (MECO) Model of Galactic Black Hole Candidates and Active Galactic Nuclei', pp 1-45 (in New Developments in Black Hole Research, ed. P.V.Kreitler, Nova Science Publishers, Inc. ISBN 1-59454-460-3, novapublishers.com) RL06 astro-phys/0602543

Romanova, M., Toropina, O., Toropin, Y., & Lovelace, R. (2003) Magnetohydrodynamic Simulations of Accretion Onto a Star in the Propeller Regime, Astrophysical Journal, 588, 400 RTTL03

Romanova, M., Ustyugova, A.,Koldoba, A., & Lovelace, R. (2005) Propeller Driven Outflows and Disk Oscillations, Astrophysical Journal Letters, 635, L165

Schild, R., Leiter, D. & Robertson, S. (2006) Observations Supporting the Existence of an Intrinsic Magnetic Moment Inside the Central Compact Object Within the Quasar QO957+561, Astronomical Journal, 132, 420

Schild, R., Leiter, D. & Robertson, S. (2008) Direct Microlensing-Reverberation Observations of the Intrinsic Magnetic Structure of AGN in Different Spectral States: A Tale of Two Quasars, Astronomical Journal, 135, 947

Shen, Z., et al. (2005) A Size of 1 AU for the Radio Source Sgr A* at the Centre of the Milky Way, Nature, 438, 62

Stirling A. M., et al. (2001) A Relativistic Jet From Cygnus X-1 in the Low/Hard X-ray State, Monthly Notices of the Royal Astronomical Society 327, 1273

Thorne, K. (1965) Energy of Infinitely Long Cylindrically Symmetric Systems in General Relativity, Physical Review B, 138, B251

Toropina, O., Romanova, M., Toropin, Y., & Lovelace, R. (2003) Magnetic Inhibition of Accretion and Observability of Isolated Old Neutron Stars, Astrophysical Journal 593, 472

Vadawale, S., Rao, A. & Chakrabarti, S. (2001) Spectral Differences Between the Radio-Loud and Radio-Quiet Low/Hard States of GRS 1915+105: Possible Detection of Synchrotron Radiation in X-Rays, Astronomy & Astrophysics, 372, 793V

Yuan, F., Markoff, S. & Falcke, H. (2002) NGC 4258: A Jet Dominated Low Luminosity AGN, Astronomy & Astrophysics, 383, 854

Yuan, F., Quataert, E., Narayan, R. (2003) Nonthermal Electrons in Radiatively Inefficient Accretion Flow Models of Sagittarius A*, Astrophysical Journal 598, 301

Yusef-Zadeh et al., 2006, in VI Microquasar Workshop: Microquasars and Beyond, Sept. 18-22, (2007) Flaring Activity of Sgr A*: Expanding Hot Blobs, Como, Italy, astro-ph/0612156

Yusef-Zadeh et al. (2006) Flaring Activity of Sgr A* at 43 and 22 GHz: Evidence For Expanding Hot Plasma, Astrophysical Journal 650, 189

Yusef-Zadeh et al. (2008) Simultaneous Chandra, CSO and VLA Observations of Sgr A*: The Nature of Flaring Activity, Astrophysical Journal, 682, 361

Zaumen, W. T. (1976) Pair Production in Intense Magnetic Fields, Astrophysical Journal, 210, 776

APPENDIX

A. ECO Models

An "eternally collapsing object" ECO is a gravitationally compact mass supported against gravity by internal radiation pressure (Mitra 2006). In its outer layers of mass, a plasma with some baryonic content is supported by a *net* outward flux of momentum via radiation at the local Eddington limit L_{Edd} given by

$$L_{Edd,s} = \frac{4\pi GMc(1+z_s)}{\kappa} \tag{6}$$

Here κ is the opacity of the plasma, subscript s refers to the baryonic surface layer and z_s is the gravitational redshift at the surface. In General Relativity z is given by

$$1 + z = 1/\sqrt{1 - 2GM/c^2R} \tag{7}$$

For a hydrogen plasma, $\kappa = 0.4$ cm$^2 g^{-1}$ and

$$L_{Edd,s} = 1.26 \times 10^{38} m(1+z_s) \quad ergs^{-1} \tag{8}$$

where $m = M/M_\odot$ is the mass in solar units.

Since the temperature at the baryon surface is beyond that of the pair production threshold and the compactness is large enough to guarantee a high rate of photon-photon collisions, (Cavaliere & Morrison 1980) there is a pair atmosphere further out that remains opaque. The net outward momentum flux continues onward, but diminished by two effects, time dilation of the rate of photon flow and gravitational redshift of the photons. The escaping luminosity at a location where the redshift is z is thus reduced

by the ratio $(1+z)^2/(1+z_s)^2$, and the net outflow of luminosity as radiation transits the pair atmosphere and beyond is

$$L_{net\ out} = \frac{4\pi GMc(1+z)^2}{\kappa(1+z_s)} \tag{9}$$

Finally, as distantly observed where $z \to 0$, the luminosity is

$$L_\infty = \frac{4\pi GMc}{\kappa(1+z_s)} \tag{10}$$

For hydrogen plasma opacity of 0.4 cm^2 g^{-1}, and a typical GBHC mass of 7 $M_\odot$ this equation yields $L_\infty = 8.8 \times 10^{38}/(1+z_s)$ erg s^{-1}. But since the quiescent luminosity of a GBHC must be less than about 10^{31} erg s^{-1}, we see that it is necessary to have $z_s > 8.8 \times 10^7$. Even larger redshifts are needed to satisfy the quiescent luminosity constraints for AGN. This is extraordinary, to say the least, but perhaps no more incredible than the $z = \infty$ of a black hole.

At the low luminosity of Eq. 10, the gravitational collapse is characterized by an extremely long radiative lifetime, τ (Robertson & Leiter 2003, Mitra 2006) given by:

$$\tau = \frac{\kappa c(1+z_s)}{4\pi G} = 4.5 \times 10^8 (1+z_s)\ \ yr \tag{11}$$

With the large redshifts that would be necessary for consistency with quiescent luminosity levels of BHC, it is clear why such a slowly collapsing object would be called an "eternally collapsing object" or ECO.

For $(1+z) > \sqrt{3}$, radiation is impeded by passage through a small escape cone such that the fraction of radiation that could escape if isotropically emitted at radius R would only be

$$f = 27\frac{R_g^2}{R^2(1+z)^2} \tag{12}$$

For very large z, $R \approx 2R_g$ and $f = (27/4)(1+z)^{-2}$.

At the outskirts of the pair atmosphere of an ECO the photosphere is reached. Here the temperature and density of pairs has dropped to a level from which photons can depart without further scattering from positrons or electrons. Nevertheless, the redshift is still large enough that their escape cone is small and most photons will not travel far before falling back through the photosphere. If we let the photosphere temperature and redshift be T_p and z_p, respectively, the net escaping luminosity is

$$L = \frac{27R_g^2 4\pi R^2 \sigma T_p^4}{R^2(1+z_p)^2} = \frac{4\pi GMc(1+z_p)^2}{\kappa(1+z_s)} \tag{13}$$

But in the radiation dominated region beyond the photosphere, the temperature and redshift are related by

$$T_\infty = \frac{T}{1+z} \tag{14}$$

where T_∞ is the distantly observed radiation temperature. Substituting into the previous equation, we obtain

$$L_\infty = (27)4\pi R_g^2 \sigma T_\infty^4 = \frac{4\pi GMc}{\kappa(1+z_s)} \tag{15}$$

and, for hydrogen plasma opacity

$$T_\infty = \frac{2.3 \times 10^7}{[m(1+z_s)]^{1/4}} \quad K \tag{16}$$

The left equality of Eq. 15 can be written in terms of the distantly observed spectral distribution, for which the radiant flux density at distance R ($> 3R_g$) and frequency ν_∞ would be

$$F_{\nu_\infty} = \frac{2\pi h\nu_\infty^3}{c^2} \frac{1}{e^{(h\nu_\infty/kT_\infty)} - 1} \frac{27R_g^2}{R^2} \tag{17}$$

B. MECO

It seems likely that GBHC are formed via stellar core collapse. One would expect the collapsing plasma to produce magnetic fields via flux compression comparable to the $\sim 10^{13-14}\,G$ found in young neutron stars. We assume that the field at the photon sphere of an ECO would be dipolar and of similar magnitude. Distantly observed dipole fields that would originate on a redshifted surface have been previously examined (Baumgarte & Shapiro 2006, Rezzola et al. 2001). Their Einstein-Maxwell equations show that the components of the dipole magnetic field strength, B at distance r from the surface are given by

$$B_r = 2F(x)\mu\cos(\theta)/r^3 \tag{18}$$

and

$$B_\theta = G(x)\mu\sin(\theta)/r^3 \tag{19}$$

where μ is the distantly observed magnetic moment, $x = r_s/2R_g$ and

$$F(x) = (-3x^3)[ln(1-x^{-1}) + x^{-1}(1+x^{-1}/2)] \tag{20}$$

$$G(x) = (6x^3)[(1-x^{-1})^{1/2} ln(1-x^{-1}) + x^{-1}(1-x^{-1}/2)(1-x^{-1})^{-1/2}] \tag{21}$$

Note that for $r_s >> 2R_g$, $x >> 1$ and both $F(x)$ and $G(x) \to 1$, while as we approach a compact MECO surface where $(1+z_s) >>> 1$, then $x \to 1^+$ and

$$F(x) \to -3ln(1-x^{-1}) = -3ln(1/(1+z_s)^2) = 6ln(1+z_s) \tag{22}$$

and

$$G(x) \to 3(1-x^{-1})^{-1/2} = 3(1+z_s) \tag{23}$$

Hence the radial component of the magnetic field at a MECO exterior surface would be given by

$$B_{r,S^+} = 12ln(1+z_s)\mu\cos(\theta)/(2R_g)^3 \tag{24}$$

while the poloidal component is given by

$$B_{\theta,S^+} = 3\mu(1+z_s)\sin(\theta)/(2R_g)^3 \tag{25}$$

Continuity of the normal components of the magnetic field would lead also to

$$B_{r,S^-} = 12\mu ln(1+z_s)\cos(\theta)/(2R_g)^3 \tag{26}$$

Following Baumgarte & Shapiro (2006) we assume that the magnetic field at the interior of the collapsing surface would be dipolar to lowest order to obtain

$$B_{\theta,S^-} = 6\mu \ln(1+z)\sin(\theta)/r^3 \tag{27}$$

Equations 25 and 27 will allow us to estimate the surface redshift from magnetic fields. The ratio of equations is

$$\frac{3(1+z_s)}{6ln(1+z_s)} = \frac{B_{\theta,S^+}}{B_{\theta,S^-}} \tag{28}$$

As noted above, a redshift of $\sim 10^8$ would be needed in order to satisfy the luminosity constraints for GBHC. But if $B_\theta \sim 10^{12-14}\ G$ at the photon sphere, then at the surface the field strength could be as large as 10^{20} G. In fact, it cannot be much larger than the quantum electrodynamically determined maximum value for a NS given by $B_{\theta,S} \sim 10^{20}$ gauss [Harding, A., 2003]. This is because surface magnetic fields much larger than $\sim 10^{20}$ gauss would create a spontaneous quantum electrodynamic phase transition associated with the vacuum production of bound pairs on the MECO surface [Zaumen 1976]. For this reason, we estimate $B_{\theta,S^+} \sim 10^{20}$ G.

At the interior surface of a GBHC, we expect the field B_{θ,S^-} to have about the magnitude that can be obtained via flux compression in a stellar core collapse. Thus for a GBHC, we expect $B_{\theta,S^-} \sim 10^{13.4}$ G, as can be estimated from Gupta, Mishra, Mishra & Prasanna (1998). For MECO objects differing in mass from GBHC, this value needs to modified by appropriate scaling. Even if the exterior field strength is not sufficient to produce bound pairs on the MECO surface the temperature there will be above the pair production threshold and there will be a pair plasma in the surface region. At the low baryon density near the surface, the interior field should be an equipartition field. Deeper within the MECO, with densities approaching nuclear density, the field could be well below equipartition. At equipartition the photon pressure in a pair plasma is proportional to B^4. It must be capable of countering the gravitational pressure, which is proportional to the mass density. At the compactness of a MECO, the mass density will scale as m^{-2}. Thus we require $B^4 \propto m^{-2}$ or $B \propto m^{-1/2}$. Incorporating this scaling and starting from a GBHC of $\sim 7M_\odot$ we estimate $B_{\theta,S^-} \sim 10^{13.4}\sqrt{7/m}$ G.

With these estimates of B_θ substituted into Eq. 28, we can iteratively solve for the redshift and find

$$1 + z_s = 1.5 \times 10^8 \sqrt{m/7} \tag{29}$$

In addition, from the equatorial exterior surface magnetic field strength of $10^{20}\ G$ we obtain

$$\mu = (2R_g)^3 B_\theta/[3(1+z_s)] \sim 2 \times 10^{30} G\ cm^3 (m/7)^{5/2} \tag{30}$$

We have found that this magnetic moment, and the spin rates given by Table 1, Eq. 6 give the MECO model a good correspondence with observations of spectral state switches and the radio luminosities of jets for both GBHC and AGN (RL03, RL04).

A few additional comments are appropriate here. The combination of an equipartition field at the MECO surface and a strong redshift dependence provides a measure of stability for the MECO. If the field increased for some reason, this would cause more pairs to be produced than just those required for the Eddington balance of the MECO-GBHC surface. Additional photon pressure would then cause the MECO-GBHC surface to expand. However the resultant expansion due to this process would reduce the redshift and the magnetic field thus quenching the vacuum production of bound pairs and

allowing the MECO-GBHC surface to contract. Similarly, if the surface contracted excessively, the increase of redshift would lead to a stronger field and more pair production, hence more radiation pressure to support the surface.

In contrast with neutron stars, where a relatively non-conducting crust might allow continuity of B_θ across the boundary, the surface region of a MECO would be highly conductive. Plasma in the vicinity of the surface would be subject to drift currents proportional to $\mathbf{g} \times \mathbf{B}/B^2$. It then follows from Ampere's law that the interior and exterior fields at the surface must differ. It is possible that future improvements on upper limit quiescent luminosity observations for Sgr A* will require that the surface redshift of its central MECO be larger than that which we have estimated here. However this possiblity could be easily accommodated in the MECO model because this would only require that a larger value of ratio of the MECO outer tangential surface magnetic field to the MECO inner tangential surface magnetic field be used in Eq. 28.

Finally, we note that in both GBHC and AGN, the maximum luminosity of the low-hard x-ray states and a cutoff of radio emissions from jets occurs at about 2% of Eddington luminosity. To accommodate these facts, it is necessary for the magnetic moment to scale as $m^{5/2}$, as it does in our MECO model (RL04, RL06).

C. The Photosphere

As previously discussed (RL06), if one naively assumes that the photon support for an ECO originates from purely thermal processes, one quickly finds that the temperature in the baryon surface layer would be orders of magnitude higher than the pair production threshold. The compactness then guarantees (Cavaliere & Morrison 1980) that photon-photon collisions would copiously produce electron-positron pairs, which would have the effect of buffering the temperature at about the pair production threshold. This makes the baryon surface a phase transition zone at the base of an electron-positron pair atmosphere. The decline of temperature within the pair atmosphere will eventually lead to a decrease in pair density and the occurrence of a photosphere as a last scattering surface for outbound photons. As will be shown, the escape cone at the photosphere is so small that few photons escape from there even without further scattering. The photosphere can be found from the condition that (Kippenhahn & Wiggert 1990)

$$\int_{\infty}^{R_p} n_{\pm}\sigma_T dl = 2/3 \tag{31}$$

where dl is an increment of proper length in the pair atmosphere and $n_{\pm}$ is the combined number density of electrons and positrons along the path. Landau & Lifshitz (1958) show that

$$n_{\pm} = \frac{8\pi}{h^3}\int_0^{\infty} \frac{p^2 dp}{\exp\left(E/kT\right)+1} \tag{32}$$

where p is the momentum of a particle, $E = \sqrt{p^2c^2 + m_e^2c^4}$, k is Boltzmann's constant, h is Planck's constant and m_e, the mass of an electron. For low temperatures such that $kT < m_ec^2$ this becomes:

$$n_{\pm} \approx 2(\frac{2\pi m_e kT}{h^2})^{3/2}\exp\left(-m_ec^2/kT\right) \tag{33}$$

$$= 2.25\times 10^{30}(T_9/6)^{3/2}\exp\left(-6/T_9\right)\ \ cm^{-3}$$

where $T_9 = T/10^9\mathrm{K}$.

We can express dl in terms of changing redshift as

$$dl = |dr|(1+z) = 4R_g dz/(1+z)^2 \tag{34}$$

for $R \approx 2R_g$ Substituting into Eq. 31 and using $T_\infty = T/(1+z)$ beyond the photosphere we obtain the relation

$$1.77 \times 10^{12} m(T_{\infty,9}/6) \int_{\sqrt{T_{\infty,9}/6}}^{\sqrt{T_9/6}} e^{-6/T_9} d\sqrt{T_9/6} = 2/3 \tag{35}$$

Using Eqs. 16 and 19, we have numerically integrated this equation to obtain the photosphere temperatures and redshifts for various masses. The results are represented with errors below 1% for $1 < m < 10^{10}$ solar mass by the relations:

$$T_p = 4.9 \times 10^8 m^{-0.032} \qquad K \tag{36}$$

and

$$1 + z_p = 1840 m^{0.343} \tag{37}$$

These relations, though little different from those of RL06, correct an error in our previous development of the photosphere temperature.

D. Accretion Efficiency And MECO Surface Luminosity

It is true that a MECO will eventually achieve 100% efficiency of conversion of accretion mass-energy to outgoing radiation, but the conversion takes place on the time scale of the MECO radiative lifetime. As previously discussed, accreting particles that reach the photosphere do not produce a hard radiative impact. They first encounter soft photons, then photons of ~ 1 Mev and then electron-positron pairs at the photosphere and they eventually reach the baryon surface where the net outflowing luminosity is already at the local Eddington limit rate. This provides a very soft landing in a phase transition zone among the baryons. As previously noted, the MECO can adjust to having additional mass in a time that is short compared to the time for required for any Compton enhanced photons to diffuse through the pair atmosphere from the MECO baryon surface. In effect, accreting mass that reaches the baryon layer becomes part of the MECO mass without producing externally observable radiation.

We can show that almost none of the energy of accretion is dissipated in the pair atmosphere by considering the interaction of accreting protons with electrons, positrons or photons. The number of interactions experienced by a proton passing through the pair atmosphere can be expressed generally as $n\sigma l$, where n is the number density of electrons/positrons or photons, σ the interaction cross section and l the proper length thickness of the pair atmosphere. This number multiplied by the fraction of original energy lost per interaction by an incoming proton yields the amount of energy lost in passing through the pair atmosphere.

As noted in the main text, the proper length thickness of the pair atmosphere is $\sim 8 \times 10^6\ cm \sim 10^7\ cm$. With a mean temperature of about $3 \times 10^9\ K$ in the pair atmosphere, Eq. 33 gives the number density of pairs to be $\sim 10^{29}\ cm^{-3}$. The photon density in the pair atmosphere would be about $n \sim 4\sigma T^3/(ck) \sim 10^{30}\ cm^{-3}$ where σ is the Stefan-Boltzmann constant and k is Boltzmann's constant.

The coulomb cross section would be proportional to $(e^2/2m_e\gamma v^2)^2$ where v is the speed of electron/positron relative to the proton. For an electron or positron moving at

approximately the speed of light relative to the proton, and $\gamma = (1+z_p) = 3.5\times10^5$, the cross section[8] would be about 10^{-37} cm^2. An accreting proton would then have about $n\sigma l = 10^{29-37+8} = 1$ collision with an electron or positron within the pair atmosphere. Considering that the fraction of energy transferred per collision would be of the order of the ratio of electron to proton mass, it is clear that the fractional energy loss by proton - electron/positron collisions would only be $\sim 10^{-3}$.

Photons might be somewhat more effective in absorbing accretion energy. To examine this point it is useful to examine a head-on collision between a proton and a photon in the rest frame of the proton and then transform the result into the frame at rest with respect to the photosphere. If a photon has energy $h\nu$ in the photosphere frame, it will have energy $\gamma h\nu = (1+z_p)h\nu$ in the proton rest frame. Compton scatter at 180^o will produce a backscattered photon of energy $(1+z_p)h\nu/(1+2(1+z_p)h\nu/m_pc^2)$, where m_p is the proton rest mass. For $(1+z_p) = 3.5\times10^5$ and $h\nu \sim kT \sim 4\times10^{-7}$erg this yields a back scattered photon of energy $m_pc^2/2$ as seen in the frame moving with the proton. The backscattered photon departs with an energy of about $m_pc^2/2$. As observed from the photosphere rest frame the photon moves toward the baryon surface with an energy of $\gamma m_pc^2/2 = (1+z_p)m_pc^2/2$. Comparing this to the incoming proton energy of $(1+z_p)^2m_pc^2$ relative to the photosphere, it is apparent that the fraction of proton energy transferred to a photon in a head-on collision would only be $1/[2(1+z_p)] \sim 10^{-6}$. Even this small amount of energy would be dissipated in photon-photon pair production (Cavaliere & Morrison 1980). Photons scattered at smaller angles would gain even less energy, however, we can us this result to set an upper limit on the proton energy losses in the pair atmosphere. The proton-photon interaction cross section is about $\sigma = \alpha^2(h/m_pc)^2(m_pc^2/\gamma E)/4$ where α is the fine structure constant, E is the photon energy in the photosphere rest frame and $\gamma = 1+z_p$. This yields $\sigma \sim 10^{-33}$ cm^2 and $n\sigma l \sim 10^4$ interactions with photons as a proton passes through the pair atmosphere. The fraction of energy lost to photons as a proton passed through the pair atmosphere would thus be less than 10^{-2}, which is again negligible. In addition the small escape cone would allow only about $27/(4(1+z_p)^2) \sim 5\times10^{-11}$ of the Compton enhanced photons to escape. Considering collisions with photons or electron/positrons and an escape cone as large as that at the photosphere, no more than 10^{-13} of the incoming accretion energy can escape to be observed externally. For stability, the MECO must adjust its radiation rate to accomodate a growing mass, but as distantly observed, the luminosity produced by the incremental increase of mass is negligible. For mass accretion rate $\dot{m}_\infty$ the radiated luminosity increases at a rate of about $(\dot{m}_\infty/M)L_\infty$. We conclude that the efficiency and thermal equilibrium constraints of BN06 and BN09 simply do not apply to the MECO surface.

D.1 High/Soft Spectral States

Reconsideration of the MECO surface accretion efficiency necessitates a new interpretation of the high/soft spectral states of disk accreting systems. At accretion rates above the transition to the soft state, most of the luminosity of the high/soft state must arise from the accretion disk rather than the MECO. This can occur with high efficiency corresponding to an accretion disk that can penetrate well inside what would otherwise correspond to the marginally stable orbit of a non-magnetic black hole. The inner disk of a MECO is supported in part by magnetic pressure, as previously described in RL06

[8]Note that the cross section, which is proportional to $\gamma^{-2} = (1+z)^{-2}$ decreases with depth in the pair atmosphere.

and disk accretion efficiencies can reach 42% at the photon sphere at $3R_g$. We actually found this efficiency in our empirical study (RLO2) of GBHC, but considered it possible at that time that the high state radiation might have originated on a surface. Inside the photon sphere, gravitational redshift offsets the effect on luminosity of additional radiant energy release by accreting matter.

E. Sgr A* Electron Temperatures and Spectral Parameters

The energy equation for the Bondi flow is

$$\frac{v^2}{2} + \frac{c_s^2}{\gamma_h - 1} - \frac{GM}{r} = const = \frac{c_{s,\infty}^2}{\gamma_h - 1} \tag{38}$$

where v is the bondi flow speed, γ_h the ratio of specific heats for the gas, M the mass of the central object and r the radial coordinate distance from its center. The continuity equation for a rate of mass flow $\dot{m}$ is

$$\dot{m} = 4\pi r^2 \rho v = const. \tag{39}$$

We adopt the values $\dot{m} = 3 \times 10^{-6}\ M_\odot yr^{-1} = 2 \times 10^{20}\ gs^{-1} = \pi(GM)^2\rho_\infty/c_s^3$, $c_{s,\infty} = 5.5{\times}10^7\ cms^{-1}$ (Baganoff 2003) and a specific heat ratio of $\gamma_h = 5/3$ for atomic hydrogen. Thus $\rho_\infty = 2.94 \times 10^{-23} gcm^{-3}$ and $n_\infty = \rho_\infty/m_p = 18\ cm^{-3}$ Having adopted these values, they set the Bondi radius as $2 \times 10^{17}\ cm$ and they must be entered consistently in the energy equation. We use $c_s = \gamma_h K \rho^{(\gamma_h - 1)}$, where $K = p_\infty/\rho_\infty^{\gamma_h}$ for an adiabatic flow. Using $\rho = \dot{m}/(4\pi r^2 v)$ and substituting into the energy equation produces an equation of the form

$$v^2 + Av^{-2/3}/r^{4/3} - B - C/r = 0 \tag{40}$$

where A, B and C are constants. Solutions for v for various values of r are given in Table 3. Once v has been determined, ρ can be obtained from the continuity equation, and the pressure and proton temperature can be found from the adiabatic conditions. For $\gamma_h = 5/3$, the inflow never becomes supersonic, but it very closely approaches sound speed (which is half what the free-fall speed would be) by the time the magnetosphere is reached.

For the dilute plasma at the Bondi radius, there is a relatively low frequency of electron-proton collisions. The kinetic energy gained by falling electrons is not sufficient to keep them in thermal equilibrium with the ions. Approximately half of the gravitational energy released goes into heating the ions while the electrons remain relatively cold. The electrons do gain some energy, which we can calculate, in collisions with protons. As the plasma falls by dr, the time taken is dr/v. An electron travels $v_e dt = v_e dr/v$ in this time. The number of collisions with ions in this time is the distance travelled divided by the mean free path, $1/n\sigma_c$, where $\sigma_c = (\pi e^4/E_e^2)\ln\Lambda$ is the coulomb cross-section. $E_e = (3/2)kT_e$ is the electron energy, T_e the electron temperature and $\ln\Lambda$ is the coulomb logarithm, which we assume to have the value 30. For collisions with protons which, on average, have much more momentum than the electrons, the fraction of proton energy, $(1/2)m_p v^2$, that can be transferred is approximately $2v/v_e$. Then while falling dr, an electron gains energy $dE_e = (3/2)kdT_e = n\sigma_c m_p v^2 dr$. Taking $v = (GM/2r)^{1/2}$ for both the proton thermal speed and speed of descent and substituting for σ_c ($\propto T_e^{-2}$) and n ($\propto r^{-3/2}$), this integrates to yield $T_e \propto r^{-1/2}$ and specifically,

$$T_e = 7 \times 10^{15} r^{-1/2} \quad K \tag{41}$$

yields the values in Table 3.

An electron moving with the protons at speed v ($= dr/dt$) in a magnetic field would emit cyclotron radiation at a rate $dE_R/dt = 2e^4v^2B^2/(3c^5m_e^2)$. Comparing this rate for the axial dipole field of a MECO with the mass of Sgr A* with dE_e/dt above, we find that the radiation rate would exceed the rate that electron energy is extracted from the protons for $B > 8600\ G$, which holds for $r < 5 \times 10^{13}\ cm$, and cyclotron frequencies above $14\ GHz$. Nearer the MECO at smaller axial distances and higher frequencies, the electron energy extracted from the protons in the flow is essentially all that is available for radiation. This permits a rough calculation of the luminosity generated in the polar inflow. We approximate the polar inflow geometry within the magnetosphere as a cone of lateral radius $a = r_c z/z_m(in)$ at distance z from the magnetic pole. See Figure 1. The number of electrons in the cone in axial thickness dz is $dN = n\pi a^2 dz$. Thus the rate that they can radiate is about $dL = dNdE_e/dt = n\pi(r_c/z_m(in))^2 z^2 n\sigma_c m_p v^3 dz$. Substituting for $n(z)$, $\sigma_c(z)$, $v(z), T_e(z)$ as before and using $r_c = 4.4 \times 10^{13} s_1 {-}4/3\ cm$, $z_m = 10^{15}\ cm$ from equations in Table 1, this reduces to $dL = 4.8 \times 10^{40} z^{-3/2} dz$, which integrates to give the luminosity for polar inflow to axial distance z as

$$L = 6.4 \times 10^{40} s_1^{-4/3} z^{-1/2} \quad ergs^{-1} \tag{42}$$

This last result includes an additional factor of two to account for inflow into both magnetic poles.

Where the flow is optically thin above $10^{12}\ Hz$, the Larmor frequency should strongly dominate the spectrum. This frequency is a function of the magnetic field strength, which varies as r^{-3}. Alternatively, we can say that position z in the polar axial inflow is correlated with the dominant radiation frequency as $z \propto \nu^{-1/3}$. Substituting $1.36 \times 10^{17} \nu^{-1/3}$ for z in the expression just preceding Eq. 42, one obtains

$$dL = 2.7 \times 10^{31} s_1^{-4/3} \nu^{-5/6} d\nu \qquad ergs^{-1} \tag{43}$$

hence the spectral index in the optically thin sub-mm/NIR would be -0.83 for the MECO model.